Australian Journal of Earth Sciences

An International Geoscience Journal of the Geological Society of Australia

ISSN: 0812-0099 (Print) 1440-0952 (Online) Journal homepage: www.tandfonline.com/journals/taje20

Fluid-driven HTLP metamorphism at Aberfoyle, NSW: geological and geochemical insights

K. Jessop, N. R. Daczko & S. Piazolo

To cite this article: K. Jessop, N. R. Daczko & S. Piazolo (06 Jul 2026): Fluid-driven HTLP metamorphism at Aberfoyle, NSW: geological and geochemical insights, Australian Journal of Earth Sciences, DOI: 10.1080/08120099.2026.2689624

To link to this article: https://doi.org/10.1080/08120099.2026.2689624

AUSTRALIAN JOURNAL OF EARTH SCIENCES
https://doi.org/10.1080/08120099.2026.2689624

Fluid-driven HTLP metamorphism at Aberfoyle, NSW: geological and geochemical insights

K. Jessop[a], N. R. Daczko[a] and S. Piazolo[b]

[a]Faculty of Science and Engineering, School of Natural Sciences, Macquarie University, Sydney, NSW, Australia; [b]Faculty of Environment, School of Earth, Environment and Sustainability, University of Leeds, Leeds, UK

ABSTRACT

Hot fluids in the crust are widely recognised, yet the sources and prevalence of fluid-driven metamorphism (metasomatism and advective heat transport) remain debated. Here, we document a previously unrecognised high-temperature – low-pressure (HTLP) metamorphic block at Aberfoyle, ~13 km west of the well-studied Wongwibinda Metamorphic Complex (WMC) in the southern New England Orogen, eastern Australia. This fault-bounded block comprises Carboniferous accretionary complex metasedimentary rocks and notably lacks associated igneous intrusions, providing a natural setting to isolate the effects of fluid flux. A steep metamorphic gradient from greenschist to amphibolite facies over ~1 km indicates a highly localised and anomalous heat source. The rock types and metamorphic assemblages closely resemble those of the WMC, suggesting the Aberfoyle block was laterally displaced westwards along a major fault. In contrast to the WMC, the absence of pegmatite dykes allows investigation of early-stage HTLP complex development during fluid-driven metamorphism. Structural observations reveal deformation-assisted fluid channelisation within ductile shear zones is overprinted by complex veining. Integrated geological and whole-rock geochemical data reveal localised fluid infiltration and channelised migration, with fluid–rock interaction intensifying systematically with metamorphic grade. We propose that during crustal extension, aqueous fluids derived from metamorphism of fertile lower crust were channelled up the Wongwibinda Shear Zone, advecting heat and initiating HTLP metamorphism in the upper crust. Subsequent channelised migration of S-type granitic melts in the Wongwibinda Shear Zone likely sustained HTLP conditions at Aberfoyle and along the shear zone margins.

KEY POINTS

1. HTLP metamorphism at Aberfoyle is documented for the first time.
2. Absence of intrusions isolates the role of fluid flux in HTLP metamorphism.
3. Geochemistry, mineralogy and veining indicate significant fluid flux.
4. Extension drove lower crustal metamorphism of fertile sedimentary rocks and channelised fluid flow controls localised upper crustal HTLP metamorphism.

ARTICLE HISTORY
Received 24 January 2026
Accepted 7 June 2026

KEYWORDS
high-temperature – low-pressure (HTLP) metamorphism; sub-regional metamorphism; aqueous fluids; complex veins; Aberfoyle; Wongwibinda; extension

Introduction

It is widely accepted that hydrous fluids are present at all levels of the Earth's crust and have sources ranging from infiltration of meteoric water, basinal brines (incorporation of seawater into sediment pore spaces), devolatisation of magmas (at deep to mid-crustal levels) and the release of water during various types of metamorphism (*e.g.* contact, regional, subduction, Steele-MacInnis & Manning, 2020).

Over the last 20 years numerous studies have demonstrated the importance of the availability of fluid to enable metastable metamorphic rocks to equilibrate to the prevailing metamorphic conditions (*e.g.* Austrheim, 2013; Daczko & Halpin, 2009; Ferry *et al.*, 2013; Jamtveit *et al.*, 2000). Infiltration of fluids will catalyse metamorphic reactions by affecting reaction kinetics, lowering activation energies, and facilitating mass transfer (*e.g.* Yardley & Bodnar, 2014). The links between deformation, vein formation and fluid flow are well recognised and have been documented at numerous localities (*e.g.* Bickle & McKenzie, 1987; Cox, 2007). Ductile shear zones are well-documented conduits of deeply derived fluids (Cox, 2007; Oliver, 1996). High time-integrated fluid fluxes (~10^6–10^7 cm^3/cm^2) provide fluid and energy for retrograde and prograde reactions within and adjacent to their boundaries (*e.g.* Doyle & Cartwright, 2000; Gates & Speer, 1991).

Many studies have linked metamorphic fluids to the formation of ore deposits (*e.g.* Yardley & Cleverley, 2015) and fluid activity related to subduction zones has been a major focus of research (*e.g.* Ague, 2003, 2011). Fluid movement within

CONTACT K. Jessop kim.jessop@mq.edu.au Faculty of Science and Engineering, School of Natural Sciences, Macquarie University, Sydney, NSW 2109, Australia
Supplemental data for this article can be accessed online at https://doi.org/10.1080/08120099.2026.2689624.
Editorial handling: Chris Fergusson

contact aureoles around plutons, and during regional metamorphism in compressional settings has generated research interest (*e.g.* Evans & Tomkins, 2020; Siron *et al.*, 2021). Lewerentz and Skelton (2018) and Lewerentz *et al.* (2017), studied the classical Barrovian setting and showed that the distribution of index minerals was related to veining. Excluding mid-ocean ridges, and except for work by Clerc *et al.* (2015), investigations in extensional settings are largely lacking. Here we explore the role of fluids in promoting high-temperature – low-pressure (HTLP) metamorphism during slab rollback within the New England Orogen (NEO) of Eastern Australia.

A fault-bounded block of metamorphosed Carboniferous accretionary complex rocks is exposed at Aberfoyle, in the southern NEO. This package of HTLP metamorphic rocks outcrops approximately 13 km west of the larger and better-studied Wongwibinda Metamorphic Complex (WMC; Figure 1b). The only previous mention of metamorphic rocks at Aberfoyle is by Binns (1966), who noted 'thoroughly reconstituted psammitic and pelitic hornfelses formed from Lyndhurst Beds [that] occur in the vicinity of Aberfoyle' but did not specify or map any locations.

A sequence of metasedimentary units, typical of the accretionary complex, has been mapped at Aberfoyle. From west to east, and over approximately 1 km, it shows a systematic increase in metamorphic grade from greenschist to amphibolite facies (Figure 1). A comparable sequence occurs on the western edge of the WMC at Lyndhurst-Rosewood (Figure 1b). However, unlike Lyndhurst-Rosewood, the Aberfoyle block: (1) is cut by the Aberfoyle River that provides outcrop across the metamorphic gradient; and (2) lacks the abundant pegmatite dykes that intrude the metamorphic rocks at Lyndhurst-Rosewood and elsewhere in the WMC. The nearest pluton, the Tobermory Monzogranite, lies ~2 km north of the Aberfoyle block and produces a contact aureole <50 m wide (Jessop, 2017), and a gravity survey by Danis *et al.* (2010) did not identify any buried plutons in the Aberfoyle area. Thus, the apparent high metamorphic field gradient at Aberfoyle—estimated at ~100 °C/km—cannot be attributed to direct magmatic heating.

This study is motivated by the question of how rock packages such as those at Aberfoyle attain the very local, high temperatures required to form small HTLP metamorphic complexes within vast areas of lower-grade rocks. The fact that initial field observations and geophysical reconnaissance rule out conductive heating from nearby plutons at Aberfoyle, prompts the working hypothesis that advective heating by hot aqueous fluids was the primary instigator of HTLP metamorphism. To test this hypothesis, we undertook detailed geological mapping, petrological analysis and geochemical investigation. This paper presents the first comprehensive geological framework for the Aberfoyle block, together with new mineralogical and geochemical data spanning the metamorphic field gradient. Details of thermodynamic modelling and geochronology of the Aberfoyle rocks will be published separately. Collectively, field relationships, veining architectures, and systematic links between whole-rock chemistry and metamorphic grade provide robust evidence that the advection of hot aqueous fluids through the Aberfoyle rocks was the principal local mechanism driving HTLP metamorphism.

Geological setting

The Aberfoyle area and the WMC occur within the Carboniferous accretionary complex of the NEO, an orogenic system that developed along the eastern margin of Australia during west-dipping, Carboniferous–Triassic subduction, punctuated by episodic cycles of contraction and extension driven by slab advance and retreat (Jessop *et al.*, 2019). The orogen preserves remnants of a Carboniferous continental magmatic arc, forearc basin and a large accretionary complex composed predominantly of trench-wedge turbidites and calc-silicate sediments interlayered with oceanic cherts, basalts and deep-sea sedimentary sequences (Cawood, 1982, 1983, 1984).

The accretionary complex occupies ~80 000 km^2 of eastern Australia and represents one of the most extensive lithotectonic components of the NEO (Figure 1a). Despite its size, metamorphic overprinting across the complex is generally minimal. Most units experienced only diagenesis to sub-greenschist facies conditions, reflecting burial within a relatively cold subduction–accretion environment typical of many accretionary prisms.

Within this broadly low-grade metamorphic framework, several highly localised occurrences of HTLP metamorphic rocks have been documented along the length of the orogen (Jessop *et al.*, 2020a, 2020b). HTLP metamorphic complexes record significant heating of the shallow crust (generally <10–15 km depth) and are characterised by steep metamorphic field gradients (*e.g.* Bodorkos *et al.*, 2002; England & Thompson, 1984; Flood & Vernon, 1978; Langone *et al.*, 2010; Sandiford *et al.*, 1998). Fourteen local HTLP zones have been identified within the NEO accretionary complex, collectively occupying only ~1.25% of its total area. These occurrences define two temporally distinct belts dated at approximately 300–290 Ma and 275–270 Ma (Jessop *et al.*, 2020a).

Individual HTLP complexes are extremely narrow relative to the surrounding low-grade rocks. The widest metamorphic zones containing biotite- to amphibolite-grade assemblages (~300–500 °C) are typically only 8–12 km across, whereas higher-grade amphibolite- to migmatite-facies rocks (~500–700 °C) are commonly <3 km wide where exposed (Jessop *et al.*, 2020a). The restricted width of these metamorphic belts implies exceptionally steep metamorphic field gradients. Across several HTLP zones, temperatures increase from either diagenetic or sub-greenschist conditions to amphibolite-facies assemblages over distances corresponding to apparent thermal gradients that steepen from ~20 °C km^{-1} in the surrounding low-grade rocks to ~100 °C km^{-1} within the higher-grade cores (Craven *et al.*, 2013).

Such gradients are significantly steeper than typical continental geothermal gradients (~25–30 °C km^{-1}) and are difficult to generate through conductive heat transfer alone (Sandiford & Powell, 1986; Sandiford *et al.*, 1998; Wickham & Oxburgh, 1985). Conductive heating associated with regional extension may elevate the geothermal gradient over broad areas of the deep crust, but it cannot readily account for the narrow kilometre-scale thermal anomalies and atypical metamorphic field gradients observed in the HTLP zones of the NEO. Instead, the geometry and spatial distribution of these

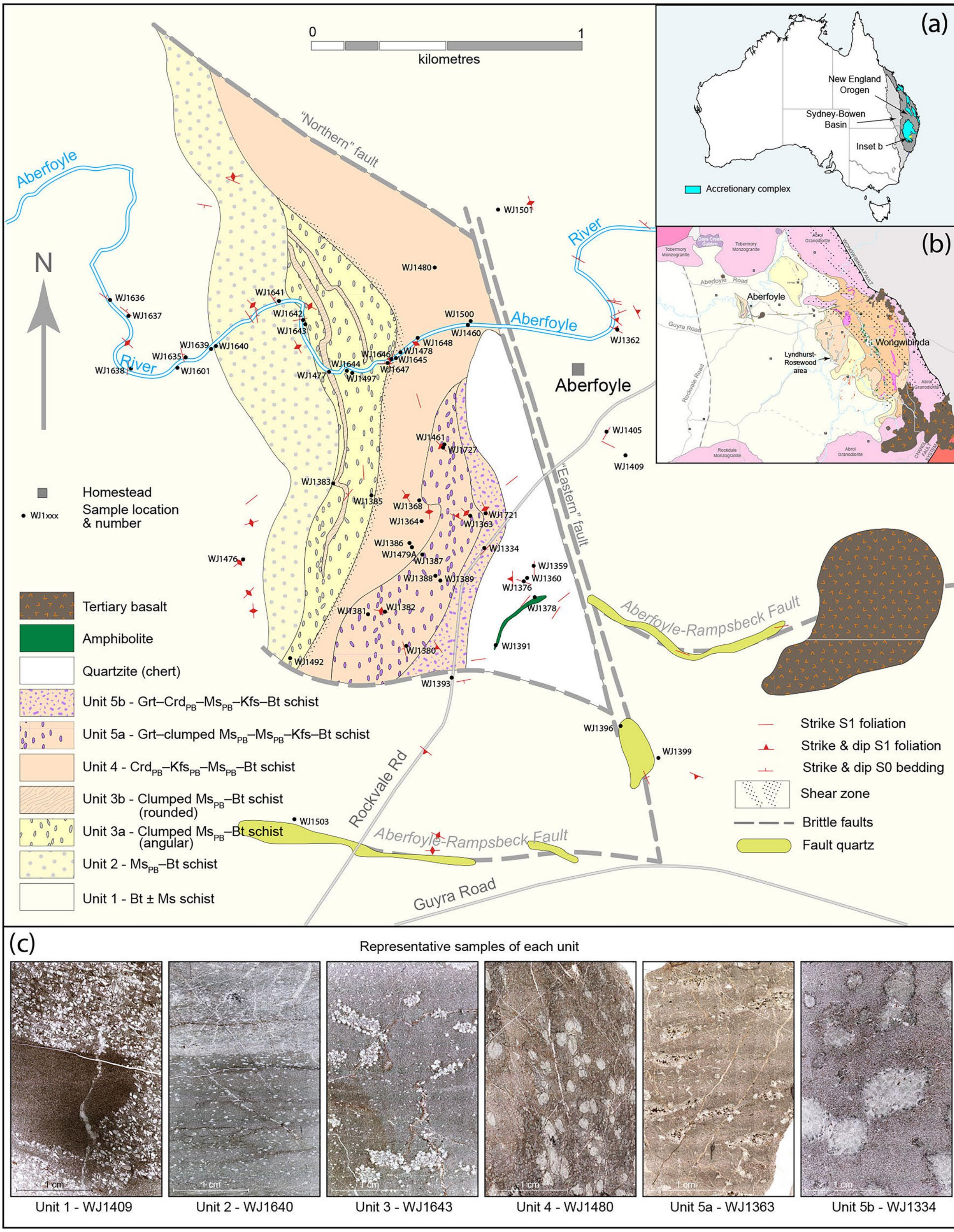

Figure 1. Geology of the Aberfoyle block showing locations of thin-sectioned samples. (a) Location of the Wongwibinda Metamorphic Complex (WMC) in northern NSW. (b) Aberfoyle to the west of the WMC. (c) Examples of changing petrology with increasing metamorphic grade. Unit 1, WJ1409 containing biotite and showing irregular contact between original pelite and greywacke. Unit 2, WJ1640 with widespread muscovite porphyroblasts in both biotite- and quartz-rich domains. Unit 3, WJ1643 containing both single porphyroblasts and clumps of muscovite. Unit 4, WJ1480 with growth of cordierite and K-feldspar porphyroblasts. Unit 5a, WJ1363 showing clumps of muscovite enclosing coarse biotite. Unit 5b, WJ1334 with large cordierite porphyroblasts.

complexes have been interpreted to reflect strongly localised heat transfer involving focused advective processes within the crust (Craven *et al.*, 2012, 2013; Jessop *et al.*, 2020b). In particular, advective transport of heat by hydrothermal fluids has been proposed to locally perturb the broader conductive thermal structure of the accretionary complex as fluids were channelled within major shear zones (Craven *et al.*, 2013; Jessop *et al.*, 2020a).

Many HTLP occurrences are spatially associated with major Permian shear zones that developed during extensional reorganisation of the orogen following termination of the Carboniferous continental arc (Jessop *et al.*, 2020b; Korsch *et al.*, 2009). This extensional phase involved crustal thinning, asthenospheric upwelling and widespread mafic magmatism, including underplating and intrusion of basaltic magmas into the crust (Landenberger & Collins, 1996). These processes likely provided important sources of heat capable of driving regional metamorphism within the deeper levels of the accretionary complex, although these levels are not presently exposed.

Sedimentary rocks within the accretionary complex were largely unmetamorphosed prior to this Permian extensional–thermal event and therefore likely retained significant volatile contents derived from hydrous minerals and pore fluids (*e.g.* Jeon *et al.*, 2012). Progressive heating of deeper accretionary complex rocks during extension would therefore have released substantial volumes of metamorphic fluid during prograde reactions. Channelised migration of such fluids provides an efficient mechanism for advective heat transport and may have played an important role in localising metamorphism within structurally focused pathways (Craven *et al.*, 2013).

The WMC represents one such HTLP occurrence. Late S-type granitoids associated with the complex record a progression from early fluid-fluxed partial melting of sedimentary protoliths to later dehydration melting and hybridisation with mantle-derived magmas (Jessop *et al.*, 2025). This evolution from highly channelised hydrothermal fluid flow to subsequent fluxing by granitic magmas indicates a transition from fluid-dominated to melt-dominated heat transport during development of HTLP metamorphic complexes.

In many HTLP localities within the NEO, later plutonism obscures the record of earlier metamorphic processes. In contrast, the Aberfoyle locality lacks igneous intrusions and therefore provides an opportunity to examine the role of fluid-mediated heat transfer during the early stages of HTLP metamorphism within the accretionary complex.

Structurally, rocks of the accretionary complex have experienced deformation associated with: (1) stacking of the subduction wedge during the Carboniferous; (2) subduction rollback, extension, and orocline formation in the early Permian; and (3) compression during the Hunter–Bowen Orogeny from the late Permian to mid-Triassic (Jessop *et al.*, 2019 and references therein).

Previous work

Binns and Richards (1965) were the first to recognise the metamorphic rocks of the WMC and undergraduate mapping studies were subsequently undertaken by numerous students from the University of New England (Alcott, 1979; Buttigieg, 1984; Fisher, 1968; Jackson, 1987; McCarron, 1989). More recently, honours and masters students from Macquarie University have investigated various aspects of the WMC (Danis, 2007; Farmer, 2017; Henson, 2000; Stuart, 2012; Teague, 2010). Farrell (1992), Craven (2015) and Jessop (2017) have completed PhD theses covering the Wongwibinda Complex.

Craven *et al.* (2012) calculated a temperature gradient of 300 to ~660 °C from low-grade metamorphic rocks to migmatites at the WMC, and a maximum pressure of 3.5 kbar (~12 km depth). In accord with Binns (1966), they concluded that peak metamorphism at the WMC preceded intrusion of the adjacent Abroi Granodiorite (Figure 1b).

Other work includes petrological studies of amphibolite pods within metamorphosed cherts and selected migmatites (Stephenson & Hensel, 1979, 1982; Vernon, 1982). Detailed structural studies of the Carboniferous sequence in the nearby Rockvale area were undertaken by Korsch (1981), and Farrell (1992) focused heavily on structural issues in the rocks adjacent to the Wongwibinda Fault.

The Lyndhurst-Rosewood area of the WMC was studied in detail in student theses by Stuart and Jessop and touched on by Farrell and Craven, but no previous work has been done at Aberfoyle. All available analytical data for both Wongwibinda and Aberfoyle are included in Supplemental data Table S1 and attributed to student authors. Other data and methods are given in the Supplemental data Tables S2–S6 and Figures S1–S9.

Results

Geology of the Aberfoyle metamorphic complex

At Aberfoyle, high-temperature–low-pressure (HTLP) metamorphic rocks are exposed across an area of approximately 2.8 km^2 (Figure 1). Outcrop is patchy, particularly away from the Aberfoyle River, but sufficient to delineate variations in rock type and structural orientation. The metamorphic package is bounded to the north, east and south by brittle faults.

Metamorphic grade increases from west to east, marked by subtle increases in grainsize and the progressive appearance of porphyroblastic minerals. Along the eastern margin, metasedimentary rocks are in contact with a band of quartzite (metachert), which contains minor pods of amphibolite. Two similar bands of quartzite–amphibolite outcrop within the main WMC, one within the zone of migmatites and one further west in the Lyndhurst-Rosewood area (Figure 1b). Stephenson and Hensel (1982) concluded that the amphibolite pods were metamorphosed oceanic basalt.

Fine beds and nodules of calc-silicate rocks occur throughout the wider Wongwibinda area. Within the fine-grained low-grade metasedimentary sequence, they are almost impossible to identify in outcrop or hand specimen and only become obvious in the highest-grade rocks (Farrell, 1992). Calc-silicates occur at Aberfoyle and have been identified by thin-section in greenschist facies rocks as well as lenses in the amphibole pods in the quartzite.

Besides the quartzite/meta-chert–amphibolite/meta-basalt unit, five metasedimentary units can be distinguished. These units all strike roughly north–south and show a systematic increase in metamorphic grade from west to east. Porphyroblasts (PB) are indicated where present. The units are as follows:

- Unit 1—Biotite ± muscovite schists
- Unit 2—Muscovite PB–biotite schists
- Unit 3—Clumped-muscovite PB–muscovite PB–biotite schists
- Unit 4—Cordierite PB–K-feldspar PB–muscovite PB–biotite schists
- Unit 5—Garnet–(cordierite or clumped-muscovite) PB–K-feldspar–muscovite PB–biotite schists

The progressive development of diagnostic metamorphic minerals from Unit 1 to Unit 5 reflects a transition from greenschist to amphibolite facies, culminating in the higher-grade quartzite–amphibolite unit at the eastern margin.

Veining, a key indicator of fluid infiltration during periods of tectonism, is ubiquitous across the Aberfoyle block. In the field, areas of dense, coarse veining are obvious, but fine veining is visible only in thin-section. A mix of simple and complex veining is found within the Aberfoyle units.

In the following, we summarise the key features of each of the mapped units based on fieldwork and thin-section analysis. Table S2 provides the location of all samples collected while those subject to chemical analysis are shown on Figure 1 and listed in Table S1. A table of samples and their associated veining is included as Table S3.

Field relationships, petrology and microstructures

Biotite schists (Unit 1)

Biotite-grade rocks are generally fine- to very fine-grained (*e.g.* Figures 1c and 2e; Figure S1c), with matrix grain sizes typically <50 µm and some quartz grains reaching ~100 µm. Coarser volcaniclastic (greywacke) protoliths outcrop in the eastern part of the unit, such as in samples WJ1409 and WJ1405, which contain relict lithic and mineral clasts ranging from ~300 µm to 1.5 mm (Figure 1c; Figure S1d, e).

The lowest-grade rocks, exposed in the west along the Aberfoyle River, are fine-grained, finely bedded, steeply dipping to overturned meta-turbidites (Figure S1a). These rocks are composed mainly of quartz, biotite and plagioclase, with the relative proportions of these minerals varying between individual beds or layers (Figure S1c). Muscovite is more abundant in quartz-rich beds than in those dominated by biotite. Fine flecks of graphite (<5 µm) are common throughout the sequence, with certain horizons particularly enriched in this mineral.

Moving eastward along the Aberfoyle River traverse, muscovite grains become noticeably coarser than other matrix minerals, reaching ~100 µm in grainsize, compared with ~50 µm for the surrounding matrix. All samples exhibit a foliation defined by the alignment of mica minerals.

The degree of veining in Unit 1 increases from west to east, becoming especially dense at the Unit 1–Unit 2 boundary. Fine quartz-only veins dominate the unit, although a few transition from quartz to biotite as they pass from quartz–plagioclase-rich layer to layers with a higher matrix biotite content (Figure 2e1; Figure S1f–g). In a limited number of samples, crystals of muscovite occur along the centre-line of slightly thicker quartz veins, even though muscovite is absent or sparse in the surrounding matrix (Figure S1i–j). As well as more intense veining at the Unit 2 boundary (Figure S1b), vein size and composition become more complex. In sample WJ1639, plagioclase is a major component of large and medium thickness veins, and large muscovite vein-crystals become more common (Figure S1h–k).

Westernmost samples WJ1636–1638 contain brittle cracks containing epidote, possibly sericite, and quartz (Figure S1l–n).

Muscovite-porphyroblast schists (Unit 2)

The appearance of large muscovite porphyroblasts marks the boundary between Units 1 and 2. Coinciding with intense quartz veining, distinctive muscovite porphyroblasts ranging from ~400 to 1000 µm are present in selective horizons, contrasting with a matrix grainsize of typically ~50 µm (with some grains up to 100 µm) (Figure 2f; Figure S2a, b, e). The porphyroblasts generally exhibit weak to strong alignment with the matrix foliation observed in all samples (*e.g.* Figure S2a). Deformation features, including muscovite 'mica fish', are evident in sample WJ1640 (Figure S2b, c).

Nearly all muscovite porphyroblasts at Aberfoyle are poikiloblastic, containing inclusions dominated by quartz ± biotite. The exception is a subset of muscovite crystals that formed within or along quartz veins, which are commonly inclusion-free (*e.g.* Figure S2f).

Veining in Unit 2 (Figure S2a, d–h) reflects the change in metamorphic grade. Fine (<100 m) quartz veins are still dominant, but thicker, up to 1 mm-wide quartz veins with coarse biotite selvedges are more common (Figure S2d, f). Complex, plagioclase-rich veins containing muscovite and K-feldspar as well as quartz and biotite are present in samples WJ1640 and WJ1642 (Figure 2f1–2; Figure S2a, g, h). The boundary of Units 2 and 3 is marked by coarse veining (Figure 2a, b; Figures S3a, b, e, f).

Clumped-muscovite-porphyroblast schists (Unit 3)

This unit is distinguished by the appearance of clumps of coarse muscovite, in addition to individual muscovite porphyroblasts. The clumped muscovite is readily visible in outcrop and hand specimen. Individual clumps typically range from 1 to 5 mm in length within a matrix grainsize of 50–100 µm and are either elongated along bedding or aligned along veins (Figure 3a–c; Figure S3c, d). In many clumps, the orientation of muscovite crystal faces differs between grains at the centre and those at the rim (Figure 3a–c; Figure S4a, b), although this feature is not universal (*e.g.* Figure S4g–h). Grainsize may also vary within a single clump.

Matrix minerals of quartz, plagioclase, and biotite surround all muscovite crystals, including those in the centre of clumps

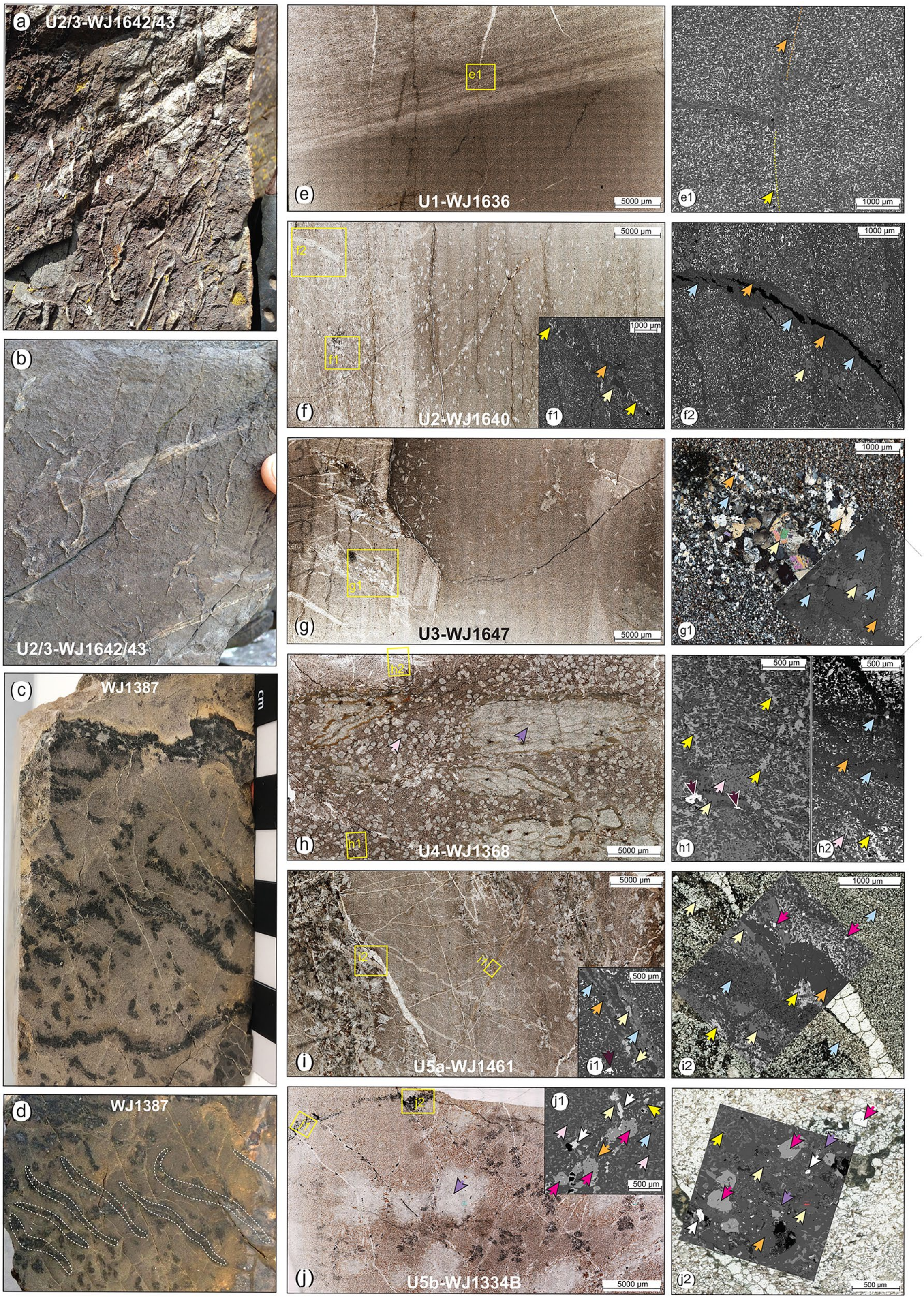

Figure 2. Veining. (a, b) En échelon veining at the boundary of Units 2 and 3. Part of geology pick handle for scale in (a), finger for scale in (b). (c, d) En échelon replacement veins of retrogressed cordierite. (e–e1) Plane-polarised light (PPL) and back-scattered electron (BSE) images of quartz to biotite veins in Unit 1. (f, f1–2) PPL and BSE images of complex veins in Unit 2. (g–g1) PPL and BSE images of complex veins in Unit 3. (h) PPL and BSE images of veining in Unit 4 (h1) network of biotite veins, (h2) network of quartz veins with minor plagioclase. (i, i1–12) PPL and BSE images of complex veins in Unit 4. (j, J1–2) PPL, BSE and reflected light images of veining in Unit 5. Arrow colours: orange, quartz; yellow, biotite; cream, muscovite; pale blue, plagioclase; pink, K-feldspar; hot pink, garnet; purple, cordierite; white, pyrite. Sample numbers on each figure.

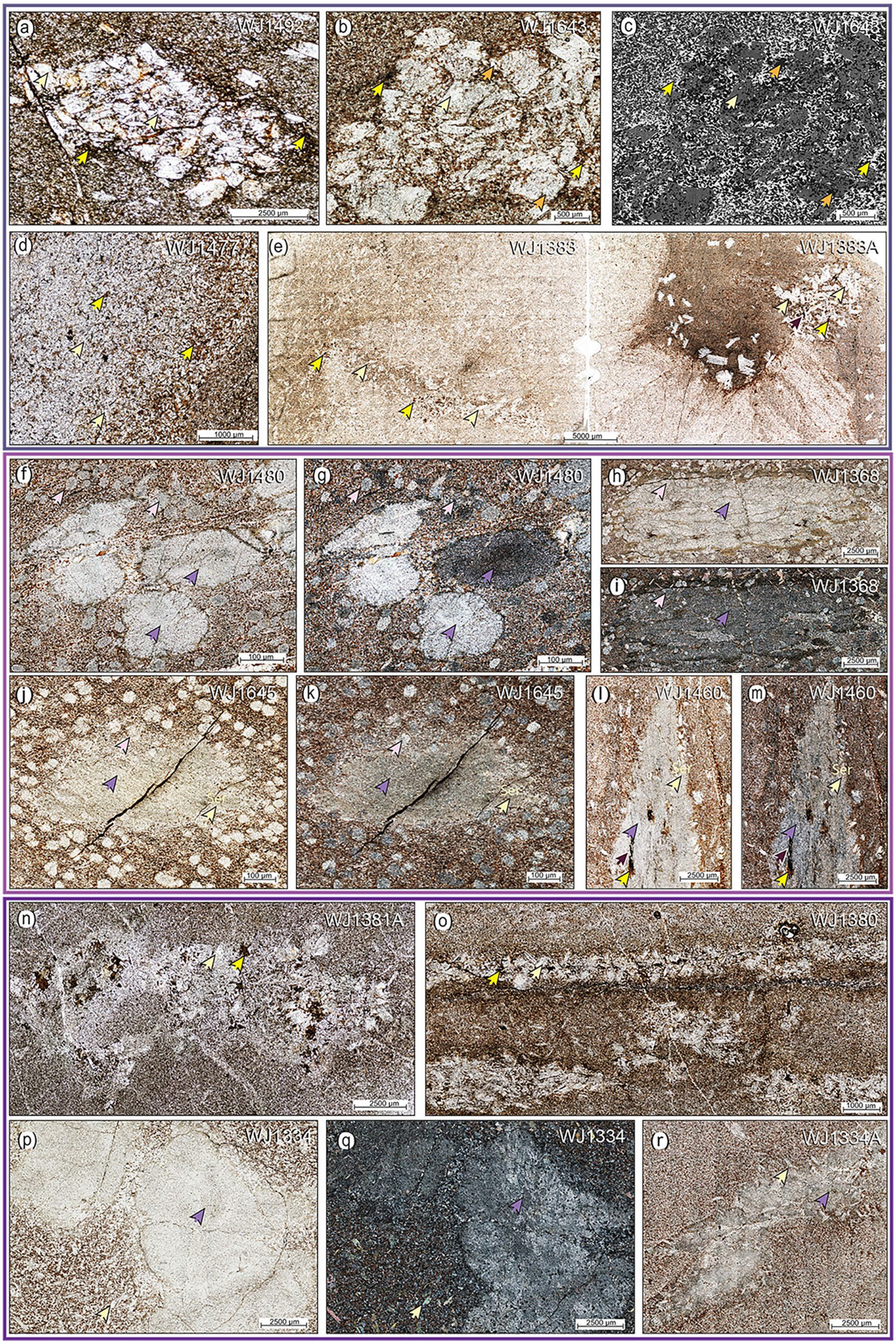

Figure 3. Clumped muscovite and cordierite. (a–c) PPL and BSE images of clumped muscovite from Unit 3 showing smaller muscovite crystals surrounded by larger ones. There is a slight increase in biotite around the clumps and some increase in quartz apparent in the BSE image (c). (d) Fine muscovite with minor biotite formed from retrogressed cordierite from Unit 3. (e) Another example of retrogressed cordierite from Unit 3 with coarse biotite in muscovite clumps. Also evident are both rounded and elongated retrogressed cordierite in the same plane (WJ1383 and 1383 A are adjoining samples). (f–g) Rounded cordierites from Unit 4. (h–i) Elongated cordierite from Unit 4. (j–k) Partly sericitised cordierite. (l–m) Strongly sericitised cordierite WJ1460. (n) Typical cordierite retrogression Unit 5a, large crystals of muscovite and large clumps of biotite. (o) Replacement vein-like cordierite retrogressed to muscovite and biotite. (p–q) Rounded cordierite Unit 5b. (r) Moderately elongated cordierite Unit 5b. Arrow colours as per Figure 2 with the addition of dark maroon, ilmenite. Sample numbers on each figure. Coloured box outlines: lavender, Unit 3; dark pink, Unit 4; purple, Unit 5.

(Figure 3a–c; Figure S4b). The abundance of matrix biotite typically increases slightly around the clumps (Figure S4f). Many muscovite clumps exhibit a roughly rectangular geometry (Figure 3a; Figure S4c).

Within Unit 3, a few horizons exhibit a distinct style of muscovite occurrence, for example, samples WJ1647 and WJ1477 (Figure 3d; Figure S4i), where very fine muscovite (~50–100 µm), biotite and quartz occur in rounded aggregates. These horizons are difficult to identify in the field, and their distribution on the geological map is inferred (Figure 1, Unit 3b). Sample WJ1383 (Figure 3e; Figure S4j) is also assigned to Unit 3b, but it differs in that it contains elongated clumps of muscovite containing larger biotite grains that are similar to those found in Unit 5 (see below). Unit 3 differs from Units 4 and 5 in that all horizons lack both K-feldspar porphyroblasts and fine-grained garnet. No other porphyroblastic minerals are present.

Most veins in Unit 3 are composed of quartz with well-developed coarse biotite selvedges (Figure S4d–e), but complex veining is more common than in Unit 2. In addition to quartz, vein minerals include plagioclase, coarse biotite, muscovite and opaques (Figure 2g1; Figure S4l, m).

Across the unit, veining is more intense in silica-rich horizons (*e.g.* Figure S4f, k). A narrow (<1 m wide) shear zone marks the boundary between Units 3 and 4, and sample WJ1385, from along the projected strike of the shear zone, shows significant deformation and quartz veining with possible evidence for multiple episodes of crack-sealing (Figure S4n, o).

Cordierite–K-feldspar-porphyroblast schists (Unit 4)

Unit 4 is characterised by the presence of cordierite, K-feldspar and muscovite porphyroblasts. Cordierite porphyroblasts range from 2.5 mm to 2 cm in size, K-feldspar from 200 µm to 1.5 mm and muscovite porphyroblasts from 200 µm to 2 mm. The matrix grainsize remains consistent with earlier units, between 50 and 100 µm (Figure 3f–i). Grain shapes vary between rounded (Figure 3f, g) and elongated (Figure 3h, i), but this may depend on the orientation of the thin-section.

Cordierite porphyroblasts contain abundant inclusions of quartz and biotite, with minor muscovite. Inclusion density is typically uniform throughout each crystal; however, some grains exhibit internal rings with fewer inclusions (Figure S5d). K-feldspar porphyroblasts are also poikiloblastic, with inclusions evenly distributed and composed mainly of quartz, with lesser biotite and minor plagioclase (Figure S5i). Where graphite is present in the matrix, it also appears as inclusions within all porphyroblast phases. In some samples, K-feldspar porphyroblasts are themselves enclosed within cordierite porphyroblasts (Figure S5a, d).

Muscovite and K-feldspar porphyroblasts appear to be in textural equilibrium when they occur together; no obvious replacement textures are observed (Figure S5b, c, f, g).

Fine, 50–200 m-wide quartz veins are present in all samples from Unit 4, and biotite selvedges are common. Veining becomes more intense in samples located towards the edges of the Aberfoyle block (WJ1480, WJ1460 and WJ1500), and coarser veining (up to 2 mm) is present. Plagioclase is present in dense veining in a silica-rich layer in sample WJ1368 (Figure S5j, k).

Muscovite and biotite commonly form on the edges of quartz veins that cut across cordierite porphyroblasts. An exception is sample WJ1480 where a quartz vein crosscuts a cordierite porphyroblast, forming an inclusion-free rim along the contact (Figure S5d, e).

Some retrogression of cordierite is apparent in this unit, but it takes a different form to that in Units 3 and 5. The smeared texture of cordierite in sample WJ1645 (Figure 3j, k) appears to be the early stages of sericitisation that is advanced in sample WJ1460 (Figure 3i–m).

Clumped muscovite or cordierite, porphyroblast schists with garnet (Unit 5a, b)

Porphyroblastic schists exposed in the eastern part of the Aberfoyle block are distinguished by abundant fine-grained garnet and the absence of K-feldspar porphyroblasts. The largest porphyroblasts are typically clumped muscovite or, less commonly, cordierite, accompanied by individual muscovite porphyroblasts. K-feldspar occurs in the matrix together with biotite, quartz, and plagioclase, which is less abundant than in other units (Figure S7a, b, e, g, i, j).

Muscovite clumps (Unit 5a) exhibit a variety of textures but consistently enclose coarse biotite crystals and opaque minerals (predominantly ilmenite, *e.g.* Figure 3n). Figure S6 illustrates the range of textures observed within these muscovite clumps. Common to all samples is their spatial association with coarse biotite (unlike the muscovite-only clumps in Unit 3). Variability exists in the proportions of fine criss-crossing *vs* larger muscovite crystals and the presence or absence of quartz halos around clumps (*e.g.* Figure S6d–h). In all samples, elongation and strong alignment of the clumps reflect either original bedding or subsequent deformation and veining (Figure S6a–c), but bedding cannot be determined in rocks of this unit.

Samples from the original discovery site on Rockvale Road (WJ1334) are unique in containing fresh or nearly fresh cordierite with no clumped muscovite (Unit 5b; Figure 3p–r). Cordierite porphyroblasts are commonly cut by veins containing biotite, muscovite, quartz and K-feldspar—a texture interpreted to be a precursor to formation of the muscovite–biotite clumps (Figure S7a, e, i). Widespread pinnitisation of cordierite is also observed.

Matrix grainsize is approximately 50 µm, with cordierite porphyroblasts and muscovite clumps up to 2.5 cm in length. Individual muscovite porphyroblasts, ranging from ~300 to ~700 µm, are distributed throughout the matrix. Garnets are commonly ≤50 µm (Figures S6i, j and S7d, h), although sample WJ1461 contains garnets up to 250 µm in an area of retrogressed cordierite (Figure S7m, n).

Complex veining is more developed in this unit, and different generations of veins are more obvious (Figure 2i1–2). Plagioclase–quartz veins in WJ1363 (Figures S6a and S7p, q) and WJ1461 (Figure S7m, n) are cut by at least one, and possibly two, episodes of later quartz veining. A thick complex vein containing large garnets (~300–400 µm), quartz, muscovite and pyrite in sample WJ1334B (Figure 2j1–2; Figure S7j–l) is cut by quartz veins also containing pyrite.

Muscovite–biotite clumps are cut by quartz and plagioclase–quartz veins (*e.g.* Figure S6a–c and S7m). However, the plagioclase is lost in the transit across the clump (Figure S6d). A thin selvedge of muscovite and biotite generally develops where fresh cordierite porphyroblasts in Unit 5b are cut by quartz veins.

Unusual 'veins' or 'tubes' that appear as black biotite in outcrop and hand specimen (Figure 2c–d; Figure S7o, r) are revealed in thin-section to be trails and clumps of muscovite with associated biotite (Figure S6b). In sample WJ1387, in addition to developing along possible bedding planes, the muscovite–biotite clumps resemble a series of stacked, 'en échelon-like' veins. These stacked veins display curvature, with vein centres rotated relative to vein tips (Figure 2d; Figure S7r), reminiscent of S–C fabrics in shear zones.

Quartzite–amphibolite unit

The quartzite–amphibolite unit also has been metamorphosed/metasomatised to amphibolite grade, as evidenced by the composition of the amphibolite pods. Hornblende–actinolite is pervasive with patchy anorthite-plagioclase remnants of original phenocrysts with minor ilmenite and titanite. Abundant anorthite-plagioclase veins commonly exhibit an extensive a calcic-clinopyroxene selvedge, together with titanite, calcite and minor muscovite, epidote, hornblende and garnet (Figure S8a–c).

The Aberfoyle quartzite (meta-chert) differs from the meta-chert units at Wongwibinda in that it is full of disseminated magnetite. Thicker (~20 cm) manganese-rich layers are prevalent in the meta-cherts at the WMC. Thin veins containing abundant garnet, magnetite, barite, barium-rich feldspars, biotite and pyrite are also found in the quartzite at Lyndhurst-Rosewood (Jessop, 2017). However, aside from magnetite, such mineralisation is absent from the unit at Aberfoyle.

Macro-structure

The HTLP rock package at Aberfoyle is truncated on three sides by brittle faults. To the east, a local, northwest–southeast-trending structure juxtaposes quartzite against biotite-grade rocks, which crop out immediately to the east. The 'Eastern' fault is defined by exposures of highly fractured and deformed metasedimentary rocks and massive recrystallised quartz with breccia clasts and vughs. It offsets a prominent west–east fault—here named the Aberfoyle-Rampsbeck Fault (Figure 1). This major fault can be traced eastward towards Wongwibinda and a kink in the Wongwibinda Fault. It differs in orientation to the north-northwest–east-southeast-trending Fishington Fault proposed by Binns (1966).

Evidence for the 'Northern' northwest–southeast-trending fault (Figure 1) includes a zone of no outcrop containing quartz float with brittle textures, and the juxtaposition of cordierite-grade rocks against biotite-grade rocks.

In the southern part of the metamorphic package, brittle deformation is again observed. A 0.5 km-wide zone of no outcrop separates the block from massive quartz outcrops to the south that define the core of the Aberfoyle-Rampsbeck Fault (Figure 1).

The main foliation in the Aberfoyle rocks is dominantly northwest–southeast (~150–270°) with a near-vertical dip, but with local variability. Where identifiable, bedding is also variable (strike 250–7° and dip 11–90°) and likely reflects folding during accretion within the subduction wedge (Figure 1). Measurements recorded during this study are included in Table S4.

Within the metasedimentary succession, dense veining is observed at the boundary between Units 1 and 2, and to a lesser extent between Units 2 and 3. A narrow ductile shear zone is exposed at the boundary of Units 3 and 4 along the Aberfoyle River. This shear zone likely extends southward, corresponding to a continuous zone of no outcrop.

Along the shear zone, muscovite porphyroblasts are deformed into mica 'fish' (Figure S10a, d, e), quartz veins are boudinaged, and fine-grained muscovite and biotite (<10 µm) occur as seams defining a new foliation (S2). S1 is interpreted as the foliation formed during deformation and metamorphism. A crenulation cleavage (S3) is also evident. Towards the margins of the shear zone, fine-grained muscovite forms rounded, elongated pods within the matrix (Figure S9b).

No contact is exposed between the metasedimentary rocks and the quartzite on the eastern boundary of the block (Figure 1). This may reflect a faulted contact. However, based on the similarity of the rock sequence at Aberfoyle and at Lyndhurst-Rosewood (WMC), it is likely that these units are either part of the original stratigraphy or were juxtaposed during formation of the accretionary complex.

Micro-structure

Outside the shear zone, the rocks at Aberfoyle generally exhibit a weak to moderate shape preferred orientation, commonly subparallel to bedding (Figure S3c, d), but typically aligned with the regional foliation (S1), which is commonly at a small angle to bedding. This orientation is most evident in the fine-grained matrix, particularly biotite, where many grains have parallel extinction, suggesting strong alignment.

Among the porphyroblastic minerals, cordierite and its replacement products show the strongest grain alignment, typically with consistent orientation. K-feldspar porphyroblasts also display a moderate preferred orientation, commonly forming short trains of crystals parallel or subparallel to the cordierite orientation. Muscovite porphyroblasts are more weakly aligned, generally showing two dominant orientations: one subparallel to the cordierite alignment and the other at a high angle to it. Muscovites that replace cordierite are randomly oriented.

Relict bedding is preserved in biotite-grade rocks but becomes increasingly obscured with increasing metamorphic grade. The alignment of porphyroblasts, particularly cordierite, may reflect original fine bedding structures.

Geochemistry

Selected samples were analysed for major and common trace elements, rare earth elements (REE) and Sr, Nd and O isotopes to investigate geochemical signatures. Given the natural geochemical variability of the volcanogenic sedimentary protoliths, and the anticipated overlap in composition between the different rock units at Aberfoyle, subtle trends correlated with metamorphic grade were specifically targeted.

Two quartzite samples and one amphibolite sample were also analysed by XRF. While of geological interest, these did not contribute meaningfully to understanding the role of fluid in driving HTLP metamorphism. Nonetheless, comparisons between the Aberfoyle quartzite and amphibolite and similar rocks from Lyndhurst-Rosewood and published datasets are included as Table S6 for completeness.

Elemental maps of samples WJ1643 (Unit 3), WJ1368 (Unit 4), and WJ1387 (Unit 5a) were obtained using a Bruker M4 Tornado Micro XRF at Macquarie University (Figure S10). Additionally, samples WJ1387 and WJ1334 (both from Unit 5) were scanned using the X-ray Fluorescence Microscopy (XFM) beamline at the Australian Synchrotron (Figure S11). Detection limits and analytical parameters are provided in the Supplemental data.

Although not all analytical results have proved useful in supporting the research objectives, they are included here for completeness.

Major and trace elements

To detect subtle whole-rock geochemical changes associated with fluid-induced mobility, major element data were recalculated as proportions of the non-silica fraction, removing the diluting effect of variable detrital quartz in the protolith. This approach reveals consistent trends: K increases with metamorphic grade, while both Ca and Na decrease (Figure 4a–b). Ba also shows a progressive increase (Figure 4f).

Similar trends to those observed for major elements are observed in trace elements. XFM maps acquired at the Australian Synchrotron for the two samples from Unit 5 at Aberfoyle (WJ1387 and WJ1334) reveal a lack of zoning of trace elements within mineral grains, but confirm that Sr is concentrated in plagioclase, and to a slightly lesser degree in K-feldspar. Rb predominates in biotite but is also present in muscovite and K-feldspar. Ba is most abundant in K-feldspar in WJ1387 but is higher in biotite in WJ1334.

Rb concentrations increase with metamorphic grade, while Sr decreases (Figure 4g). Sm and Nd values also increase from Unit 1 to Unit 4, but Unit 5 displays a reversal of this trend, with the lowest median values of both elements (Figure 4h).

Mafic elements Fe and Mg do not show any variation between the various units (Figure 4c–d). Ti trends were investigated following the results of biotite analyses (see Mineral Chemistry below). Although Ti is lowest in Unit 5, there is no pattern between the units (Figure 4e).

REEs

Chondrite-normalised REE patterns (Sun & McDonough, 1989) for all units (1–5) show broadly similar distributions, particularly within the light REE (LREE) range (Figure 5a–f). There is a consistent negative Eu anomaly across all units. Sample WJ1334, the only fresh-cordierite-bearing sample from Unit 5b, has the lowest overall REE-content but repeats the pattern of the other samples (Figure 5e–f). There is a slight change in the ratios of Yb to Lu with grade. In Units 1 and 2, there is an uptick between Yb and Lu, they are even in Units 3 and 4, but they downtick in Unit 5.

In the Aberfoyle rocks, the REEs are most likely concentrated in apatite and monazite. A plot of total-rock P_2O_5 (Figure 5g) shows a variable but generally decreasing content with grade. Averages for each unit (Figure 5h) indicate a progressive decrease that becomes more pronounced in Unit 5. (Note: sample WJ1492 from Unit 3 has anomalously high P_2O_5; it is located close to a major fault zone; and REE data are not available. It has thus been excluded from average calculations.)

Analyses of monazites contained in a single sample from each unit included selected REEs (Figure 5i). Although there is some variation between individual monazite grains, particularly with the size of the Eu anomaly, this is consistent for each sample, and the pattern across the units is close to identical.

Isotopes

Three isotopic systems were used to investigate the sequence at Aberfoyle; two radiogenic (Rb–Sr, Sm–Nd) and one stable (O). A background on the significance of these isotope systems is included in the Supplemental data. The key difference between radiogenic and stable isotopes is that the former rely on radiogenic decay from an isotope of one element into a different isotope of another element, while the latter is affected by the kinetics and bonding strength of different isotopes under varying temperature conditions.

In the three isotope systems investigated, an increase in $^{87}Sr/^{86}Sr$, a decrease in $^{143}Nd/^{144}Nd$ and an increase in $\delta^{18}O$ are evident with increasing grade (Figure 6a–f).

Rubidium–Strontium (Rb/Sr)

Within the Rb–Sr system, the $^{87}Rb/^{86}Sr$ and $^{87}Sr/^{86}Sr$ ratios reflect the general increase in Rb and decrease in Sr with metamorphic grade (Figure 4g).

A plot of $^{87}Sr/^{86}Sr$ against $^{87}Rb/^{86}Sr$ produces a striking alignment of values resembling an isochron with an age of 365.25 Ma. More exact alignment is obtained by breaking the data into three groups resulting in ages of 358.24 Ma, 337.22 Ma and 302.17 Ma (Figure 6a), all consistent with the duration of the Late Devonian–Carboniferous Currabubula–Connors continental arc (Jessop *et al.*, 2019). However, such isochrons have been recognised as mixing lines (Faure & Hensing, 2005, p. 359–360) and have been designated as 'fictitious isochrons'.

Samarium–Neodymium (Sm/Nd)

$^{143}Nd/^{144}Nd$ neodymium isotope ratios have a decreasing affiliation with metamorphic grade. Conversely, $^{147}Sm/^{144}Nd$ ratios vary little between the units (Figure 6b).

Mixing lines between two components (*e.g.* crustal and mantle sources) were developed by Langmuir *et al.* (1978) as a plot

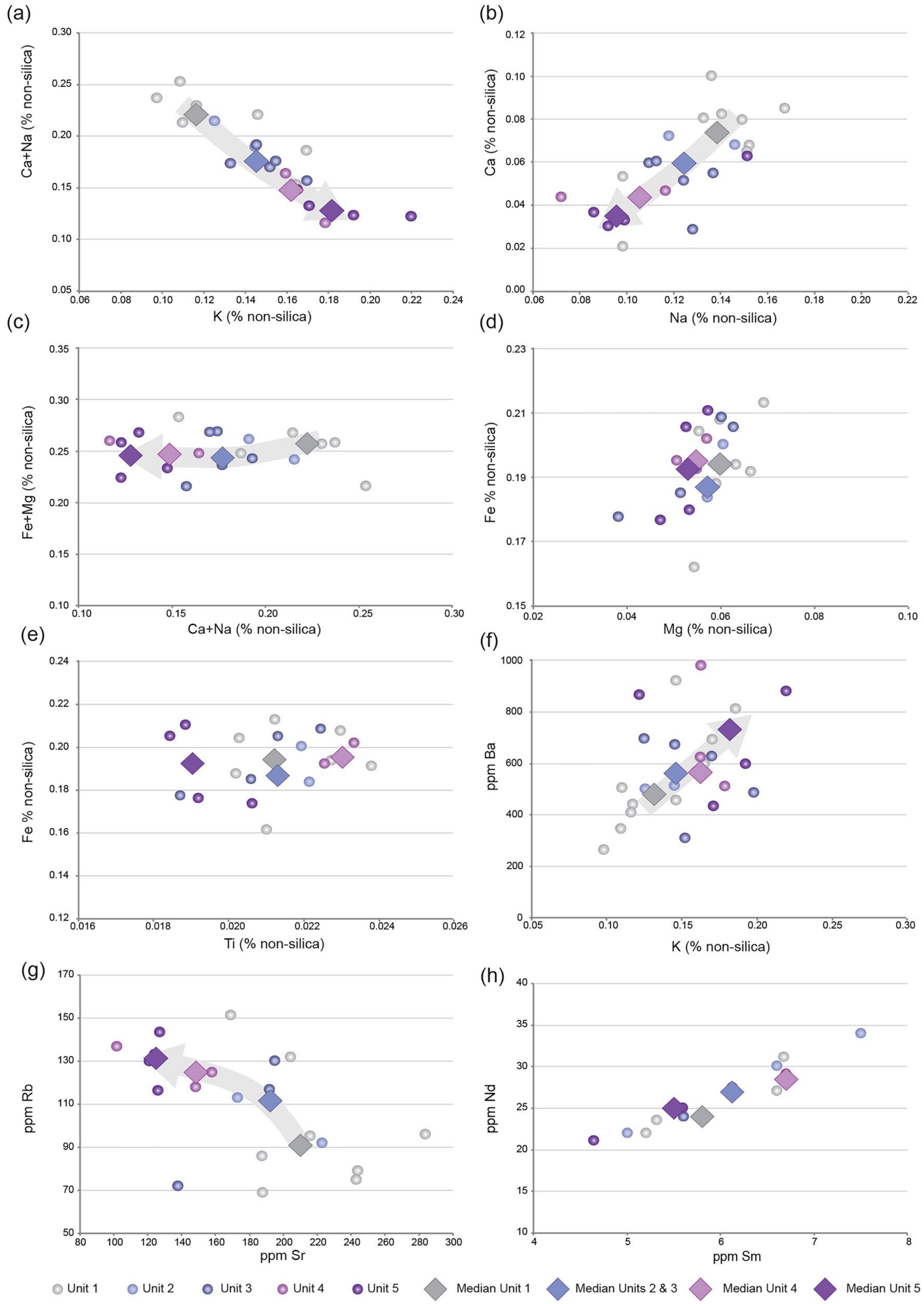

Figure 4. Major and trace elements. Plots of major elements adjusted to exclude silica and selected trace elements. Median values calculated for each Unit at Aberfoyle reveal overall element trends. Soft grey arrows highlight element relationships that change consistently with metamorphic grade.

of $^{143}Nd/^{144}Nd$ against $^{87}Sr/^{86}Sr$ values. Our data superimposed on these mixing lines (Figure 6e) form a line, but one that is not consistent with a two-component mix between Global Average Crust and mantle. A curve can be fitted to the data, but it assumes a more juvenile crustal component such as that of eastern Australia.

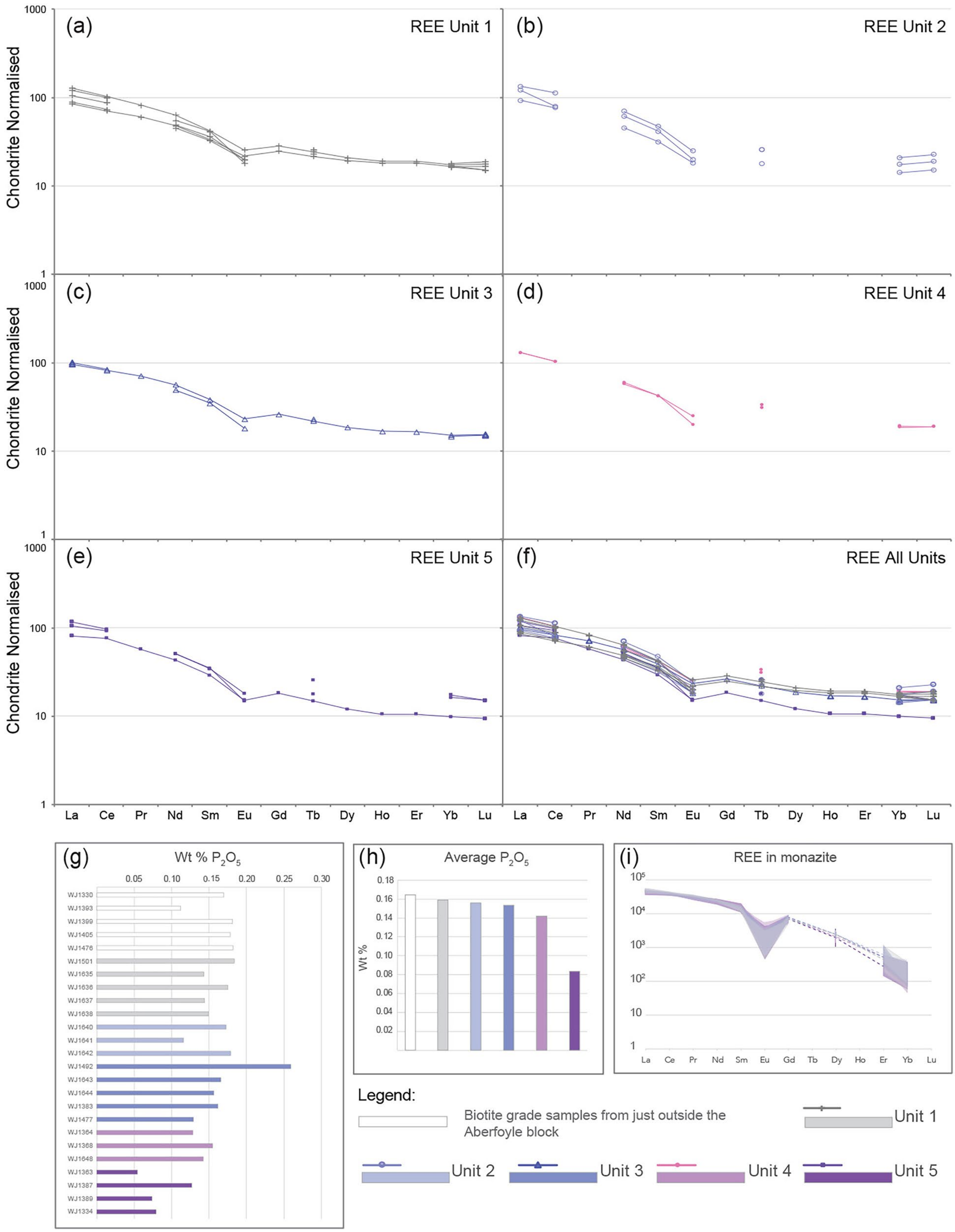

Figure 5. Rare earth elements (REEs). (a–f) Chondrite normalised whole-rock REE profiles for each of the metamorphic units. Note the missing values are from samples tested by neutron activation analysis. (g, h) P_2O_5 values are linked to REE-carrying monazite and apatite contents of the units. (i) REE values from monazites do not vary between the units.

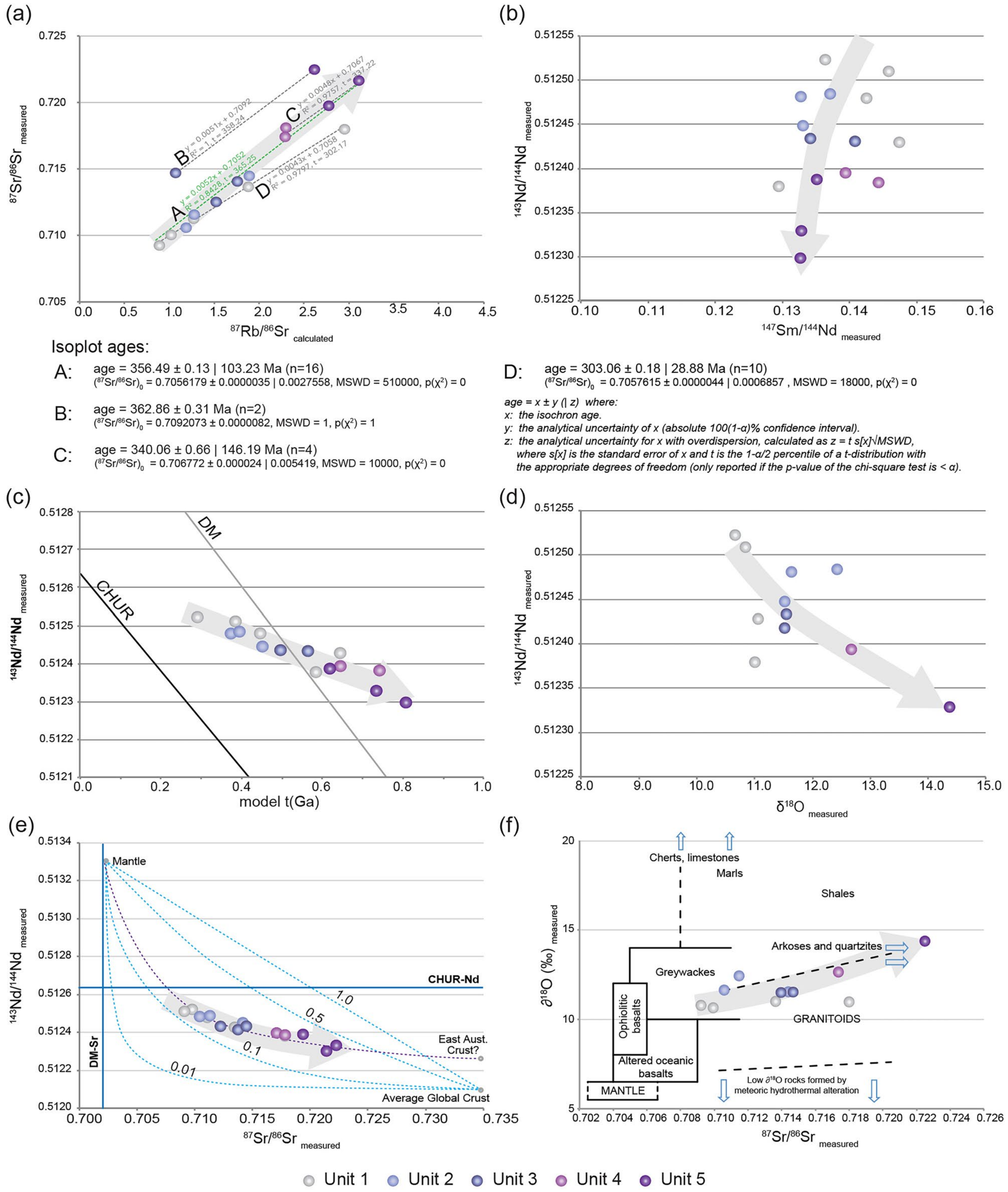

Figure 6. Isotopes. (a) Rb–Sr isotopes form 'fictitious isochrons' that correspond with feasible deposition ages but also have a general relationship with metamorphic grade. (b) $^{143}Nd/^{144}Nd$ shows a decrease with grade while $^{147}Sm/^{144}Nd$ has little variation. (c) Model ages generally increase with metamorphic grade. (d) $\delta^{18}O$ increases with grade. (e) Mixing lines after Faure and Hensing (2005). (f) O and Sr isotope plot after Rollinson (1993, p. 279).

Model ages calculated from Sm–Nd isotopic data vary from 810 to 290 Ma with a general trend for higher-grade metamorphic rocks to produce older ages (Figure 6c).

Oxygen ($\delta^{18}O$)

Although fewer samples were analysed for oxygen isotope ratios than for Sr and Nd, results show $\delta^{18}O$ also increases with metamorphic grade (Figure 6d, f).

Mineral chemistry

The compositions of various minerals within the lithological units at Aberfoyle have been investigated. Muscovite and biotite in Units 1–5 at Aberfoyle were probed to ascertain any differences in composition that may relate to prograde or retrograde processes. Comparisons were also made between plagioclase in veins and matrix.

Cordierite analyses in samples from Units 4 and 5 and garnet analyses from Unit 5 at Aberfoyle are compared with the compositions of cordierites and garnets in similar rocks from the Lyndhurst-Rosewood area and a selection of migmatites from the WMC (Craven, 2015; Farrell, 1992; Jessop, 2017; Stuart, 2012). (Supplemental data, Tables S7 and S8).

Biotite and muscovite

Figure 7 plots EMP analysis of biotite and muscovite from Units 1–5 at Aberfoyle. Plots of tetrahedral Al *vs* Ti and Mg against Fe show subtle shifts in chemistry of the micas.

Biotite

There is a general increase in tetrahedral Al in matrix biotite as metamorphic grade increases (Figure 7d). Similarly, Mg content of matrix biotite decreases with metamorphic grade (Figure 7h). There is no obvious change in Fe content (Figure 7h).

Biotite in cordierite and in clumps of muscovite has a lower Ti than the equivalent matrix biotite in all units (Figure 7b, c). Biotite in muscovite clumps in Unit 5 has increased Mg in relation to matrix biotite (Figure 7g). This is not the case with biotite in muscovite clumps in Unit 3 (Figure 7e).

Muscovite

There is a subtle decrease in both Mg and Fe in muscovite in the matrix or single porphyroblasts with increasing metamorphic grade (Figure 7p). Generally, the composition of muscovite does not vary between the matrix and single porphyroblasts, but a slight decrease in Ti in muscovite in clumps appears in Units 3 and 5 (Figure 7i, k).

Feldspars

Feldspar compositions generally do not show any clear patterns with grade. Plagioclases from Unit 1 have an andesitic composition ($An_{32–43}$) and plagioclase from Unit 5 clusters between An_{17} and An_{20}, but there is considerable overlap in compositions between the units within the oligoclase range (Figure 8a, b).

K-feldspars are predominantly perthitic orthoclase with a few perthite outliers. Of note is that SEM analyses of K-feldspars from Units 4 and 5 all show significant traces of Ba. This has also been noted in K-feldspars from the Lyndhurst-Rosewood area.

Average feldspar compositions for each unit show a subtle change with higher K in K-feldspar in Unit 3, decreasing to Unit 5 (Figure 8c). K-feldspar results for Unit 1 are from samples outside the HTLP block that have experienced minimal metamorphism. Average plagioclase compositions appear to indicate a subtle drop in Ca and increase in Na with grade. The exception is Unit 4 (Figure 8d). Average composition of plagioclase in veins is only slightly different to that in the matrix, although there are some exceptions in Unit 4.

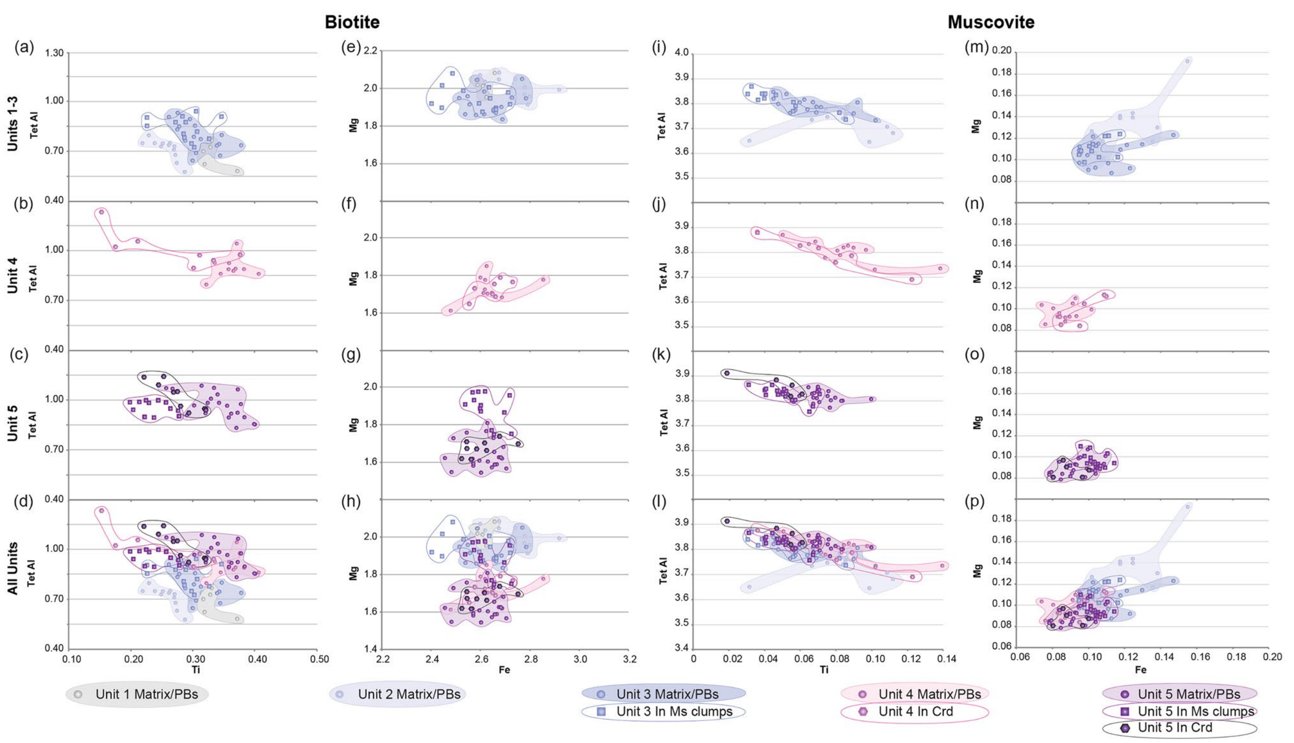

Figure 7. Biotite and muscovite mineral chemistry. Plot differentiates between biotite and muscovite in porphyroblasts, clumps and in matrix. Units 1–3 are grouped owing to paucity of porphyroblasts in lower-grade units. Trends are discussed in the text.

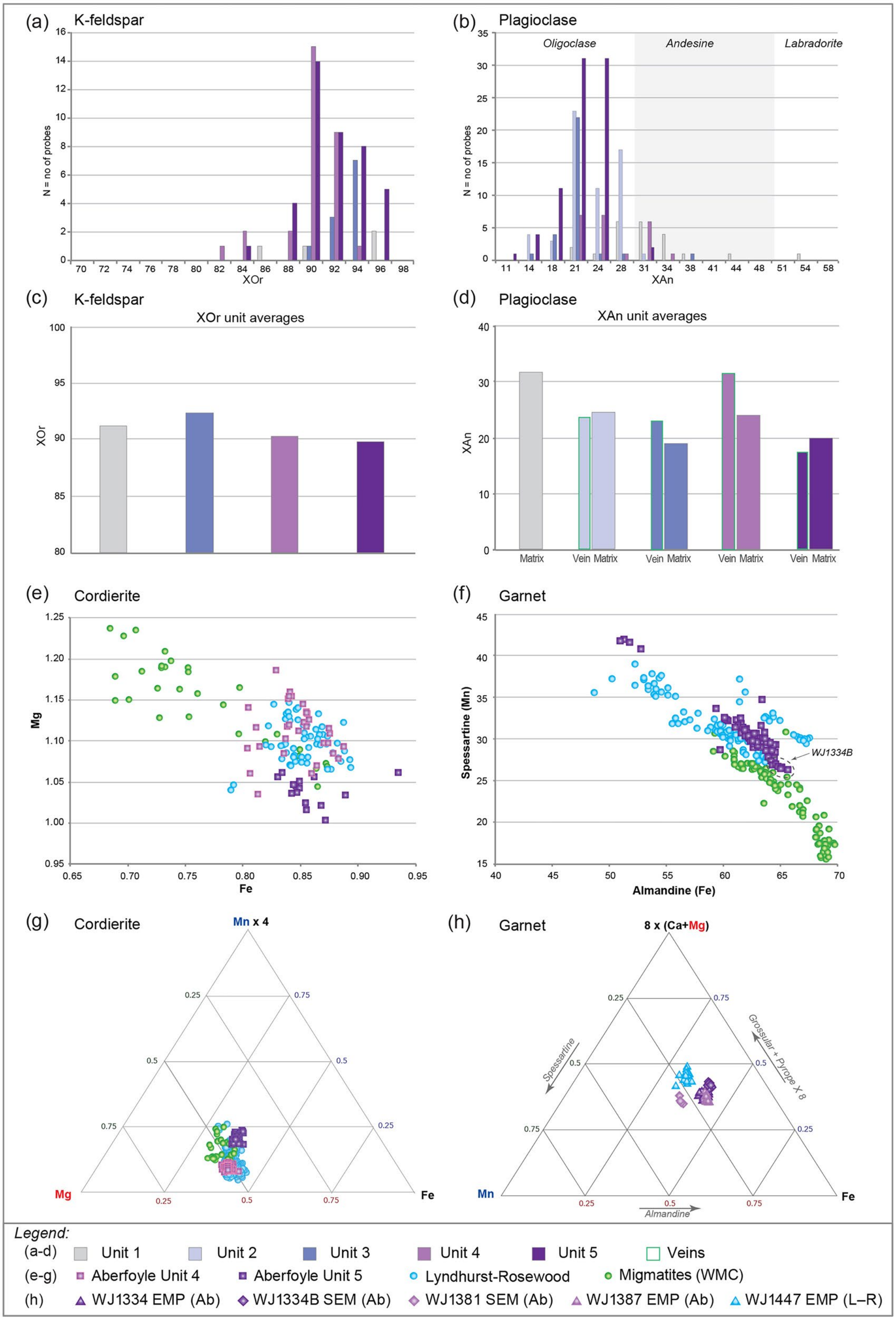

Figure 8. Feldspar, cordierite and garnet mineral chemistry. (a, b) Histograms of the frequency and chemical distribution of K-feldspar and plagioclase. (c) Averages for K-feldspar data from (a). (d) Averages for plagioclase data from (b) separating results from veins and matrix. (e) Cordierite mineral chemistry from Units 4 and 5 at Aberfoyle compared with cordierites from Lyndhurst-Rosewood and migmatites of the WMC. (f) Garnets from Unit 5 compared with those from Lyndhurst-Rosewood and migmatites of the WMC. Note similarity to migmatites of garnets from the vein in sample WJ1334B. (g) Triangular plot of data from (e) to compare Mn content (Mn multiplied by 4). (h) Triangular plot of Aberfoyle and Lyndhurst-Rosewood garnet data only (Ca + Mg multiplied by 8).

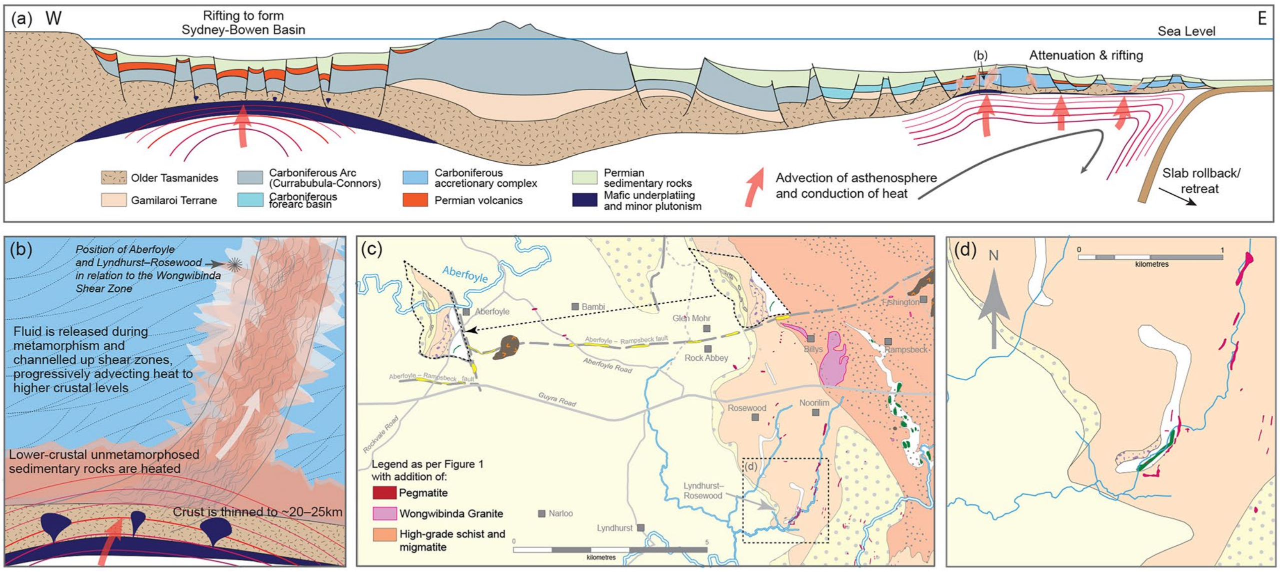

Figure 9. Proposed model. (a) Cartoon east–west section through the New England Orogen during slab rollback of the early Permian. Attenuation and rifting lead to crustal thinning, upwelling of mantle asthenosphere, decompression melting, underplating and heating of the lower crust from the mantle advection. (b) Heating and metamorphism of young, fertile metasedimentary rocks release aqueous fluids that migrate up shear zones and percolate into adjoining rock packages. (c) Proposed relocation of the Aberfoyle block to the edges of the Wongwibinda Shear Zone by reversing 8–9 km of sinistral movement along the Aberfoyle-Rampsbeck Fault. Sheared granites that currently outcrop along the Aberfoyle-Rampsbeck Fault (Figure 1b) are moved eastwards off the diagram. (d) Detail of the geology of the Lyndhurst-Rosewood area showing location of porphyroblastic cordierite, garnet schist adjacent to the meta-chert. Note that outcrop is sparse outside the creeks.

Cordierite

Cordierites from Aberfoyle contain between 2 and 7 wt% Mn in the metal cation site, while Mg ranges from 48 to 57 wt% and Fe from 34 to 45 wt%. There is a strong overlap in the composition of cordierites from Aberfoyle and Lyndhurst-Rosewood, particularly those from Unit 4 (Figure 8e). Cordierites from Unit 5b, the unit adjacent to the quartzite–amphibolite, have a higher Mn and lower Mg content than those from Unit 4 (Figure 8g). Two samples from Lyndhurst-Rosewood also have significantly higher Mn, and these samples are correspondingly close to the quartzite in that area (Figure 8g; note that Mn content has been multiplied by four to enhance visibility on the graph).

Electron microprobe analysis of cordierite in migmatites from the WMC is only available for limited samples. Mn content is variable, but generally higher than in cordierites from Unit 4 and the majority of Lindhurst-Rosewood samples. Migmatitic cordierites trend towards higher Mg and lower Fe, although there is some overlap with cordierite from both Units 4 and 5b at Aberfoyle (Figure 8e, g).

Garnet

Similarly, the garnet chemistries of the Aberfoyle and Lyndhurst-Rosewood samples also overlap (Figure 8f). Both are strongly Mn-rich (spessartine), but the Aberfoyle garnets contain slightly more Fe and less Mg and Ca than those from a similar unit at Lyndhurst-Rosewood (Figure 8h). In the metal cation site, Aberfoyle garnets contain 50–64 wt% Fe, 26–42 wt% Mn, 4–7 wt% Mg and 1–2 wt% Ca (Figure 8h, note Ca + Mg have been multiplied by 8 to enhance visibility).

Garnets from migmatite samples from the WMC progress towards lower Mn and higher Fe (almandine). For a given Fe content, Aberfoyle garnets contain more Mn than the majority of those from the general Lyndhurst-Rosewood area (Figure 8f). Garnets from the vein in sample WJ1334B (Figure 9j–l) are the most Fe-rich of the garnets from Aberfoyle (Figure 8f, h).

Discussion

The scale of the metamorphic field gradient and stratigraphic progression of metasedimentary units at Aberfoyle is almost identical to that exposed on the western side of the quartzite at Lyndhurst-Rosewood (Figure 9d). In both areas, a systematic increase in metamorphic grade occurs adjacent to a quartzite unit containing pods of amphibolite, strongly suggesting that Aberfoyle, like Lyndhurst-Rosewood, originally occupied the margin of the Wongwibinda Shear Zone (WSZ, Figure 9c). As such, the rocks at Aberfoyle were exposed to fluxes of fluid channelled up the WSZ in an open-system, extensional environment.

Dipple and Ferry (1992) assessed the volume of water released by metamorphism of pelitic rocks and the likely fluid flow focused along a shear zone. They concluded that if rocks at 15–25 km depth in the crust released just a conservative 2% H_2O that flowed up ductile faults, the metasomatism associated with the fluid channel should occupy about 1% of the crust. Using QGIS, the Carboniferous accretionary complex of the NEO has a calculated outcrop area of ~80 000 km$^{2.}$ The exposed areas of amphibolite facies HTLP metamorphism in the NEO similarly total just over 1000 km^2, or 1.25% of the accretionary complex, a result that is consistent with the above calculations.

Fluid ingress, reaction, metamorphism and egress at Aberfoyle occurred in a ductile regime along porous horizons created by deformation dilatancies and more permeable lithological horizons. Veins record the latest stages of deformation and give us some indication of fluid composition as the environment cooled and became brittle. Multiple phases of veining are present, and it is not possible to categorise these, as both deformation and fluid influx likely occurred in pulses. However, thin, straight quartz veins that cut earlier more complex veins are mostly likely a later overprint that occurred during the following tectonic contraction in the latest Permian–early Triassic.

Metamorphism through open-system fluid migration

Fluid flux through the Aberfoyle sequence triggered extensive fluid–rock interaction, resulting in metasomatism sensu Ague (2017), whereby chemical exchange was open at the scale of the rock package. Whole-rock geochemical data show systematic changes with increasing metamorphic grade, including enrichment in K, Rb and Ba, and corresponding depletion in Ca, Na and Sr, while total Fe and Mg remain approximately constant.

These trends indicate the introduction and removal of fluid-mobile elements. Petrographic observations corroborate this interpretation: muscovite and K-feldspar porphyroblasts become increasingly abundant with grade, while plagioclase diminishes in the matrix.

Trace-element mapping confirms that Rb is hosted primarily in biotite, whereas Sr resides mainly in plagioclase (and to a lesser extent K-feldspar). Progressive increases in median Rb and Ba, and decreases in Sr, reflect the growing dominance of biotite and K-feldspar over plagioclase as metasomatism intensifies. Increasing Rb contents perturb the Sr isotopic system, with the highest-grade rocks showing the greatest disturbance, consistent with more sustained fluid flux.

Mineral chemistry is consistent with, an open system, but given the proposed pulsed nature of fluid input, some local reactive environments may develop. In Units 4 and 5, biotite associated with cordierite is depleted in Mg relative to lower-grade units, consistent with Mg uptake by cordierite. Following cordierite breakdown, biotite within muscovite clumps becomes Mg-enriched again. Ti decreases, and tetrahedral Al increases with progressive metasomatism, compatible with repeated, coupled prograde–retrograde reactions occurring within a single evolving fluid system (*e.g.* Dipple & Ferry, 1992).

Similar processes may explain muscovite clumps in Unit 3, where breakdown textures suggest transient formation of a simple porphyroblast, possibly andalusite. Although andalusite is not preserved, its brief stability is consistent with short-lived heating events prior to cooling in the presence of the same fluid. The subtlety of the chemical changes suggests that retrogression did not require a chemically distinct later fluid but occurred during waning stages of the same fluid flux.

Syn-tectonic fluid flow

Deformation enhances permeability by generating porosity networks, including grain-scale dilatancies, linked vein systems and fractures along rheological boundaries (Ferry, 1988; Ferry & Dipple, 1991; Fusseis *et al.*, 2009; Ingebritsen *et al.*, 2006). These mechanisms are well developed within the Aberfoyle HTLP sequence.

All units above biotite-grade at Aberfoyle have some degree of foliation defined by aligned biotite and porphyroblasts. Biotite-rich layers exhibit ductile deformation forming well-foliated fine-grained schists, whereas quartz-rich layers fracture more readily, as evidenced by higher proportions of veining. With increasing metamorphic grade, foliation intensifies, and vein density and complexity increase, indicating enhanced fluid flux and higher temperatures. En échelon veins and replacement veins defined by aligned porphyroblasts provide strong evidence for syn-tectonic fluid infiltration.

Cordierite porphyroblasts commonly display extreme elongation and occur along deformation-related cracks, forming replacement veins consistent with growth along fluid pathways (Bons & Gomez-Rivas, 2020). Sample WJ1387 (Unit 5a) preserves particularly clear evidence of fluid flow, with cordierite (now retrogressed to muscovite clumps) concentrated along oriented crack networks. Higher abundances of metamorphic indicator minerals and vein networks at lithological and unit boundaries further suggest that fluid ingress was focused in high-stress regions.

The S–C fabric observed locally can be interpreted as an extensional crenulation cleavage (Passchier, 1991), consistent with deformation under trans-tensional conditions. In this regime, fluids were able to migrate both along minor shear zones and faults, and through channelised porous flow and subcritical cracking within the metasedimentary sequence.

Sanislav *et al.* (2020) have shown that deformation of cordierite creates cracks that allow fluid infiltration and replacement by muscovite and biotite without a change in *P*–*T* conditions. Muscovite–biotite clumps in Unit 5a are interpreted as the hydrated replacement products of cordierite preserved in Unit 5b. The coexistence of both fully preserved and replaced cordierite in this unit can be explained by deformation occurring at the same time as fluid flux.

Kilometre-scale heat advection by fluxes of hot fluids

Whether metamorphic fluids can transport heat over significant distances remains debated. Ferry (1994) demonstrated that fluids moving through networks of quartz veins can transfer heat, isotopes and chemical species, whereas Yardley (2013) argued that at depths where fluids are near-lithostatic pressure, irreversible escape limits fluid flux. However, Yardley acknowledged that strongly channelised flow could overcome these constraints. We note that the common observation of exhumed metamorphic rocks that display limited retrogression argues strongly that fluid released during dehydration reactions and prograde metamorphism is lost from the source rocks, presumably migrating upwards in the crust.

Subsequent studies support the effectiveness of focused fluid flow. Evans and Tomkins (2020) showed that prolonged channelisation can produce high fluid–rock ratios, such that chemical potentials are buffered by the fluid rather than the rock. Numerical modelling by Tian *et al.* (2018) further demonstrated that transient temperature increases of >200 °C can be sustained for up to 10^4 years within tubular fluid conduits.

Multiple generations of veining are present throughout the sequence at Aberfoyle, although their relative timing is not always clear and likely underestimates the total volume of fluid movement. Importantly, veins of different mineralogy record fluids with different thermal capacities acting simultaneously at the outcrop scale, reinforcing the interpretation of spatially and temporally variable, pulsed flow. Taken together, these observations favour a model of locally pulsed but regionally sustained fluid flux.

The progressive increase in $\delta^{18}O$ with metamorphic grade is consistent with heating in a fluid-rich environment. Fluids generated by dehydration reactions of muscovite and biotite in accretionary complex lithologies at depth would be expected to have similar initial $\delta^{18}O$ values to low-grade rocks at Aberfoyle. However, isotopic exchange is enhanced at higher temperatures, leading to progressively $\delta^{18}O$ enriched isotopic compositions, with stronger ionic bonds, replacing more volatile ^{16}O, in rocks that have experienced a more sustained and hotter fluid flux.

The influx of K and Rb is likewise consistent with liberation of these elements during breakdown of K-bearing phases at depth. In contrast, REEs show little variation in pattern across the sequence, indicating that the fluids did not carry REE-mobilising ligands and that REE largely remained rock-buffered. Subtle variations in Nd isotopes are present but cannot be uniquely linked to metamorphic processes.

A model for sub-regional HTLP metamorphism

We envisage a crustal-scale tectonic system in which extension led to metamorphism of the lower crust and structurally focused fluid flow through the middle and upper crust (Figure 9a). Deep heating occurred at the base of the crust during regional tectonic extension of the NEO, as evidenced by widespread emplacement of S-type granite suites (Craven *et al.*, 2013; Jessop *et al.*, 2020b, 2025). Crustal thinning during early Permian extension provided the thermal driver for prograde metamorphism of fertile Carboniferous accretionary prism sedimentary rocks at depth. Aqueous fluids were generated from dehydration reactions in these previously unmetamorphosed rocks, and the WSZ provided a major local conduit for fluid flow. Fluids ascending from deeper levels advected heat and mobile elements into higher structural levels, initiating and sustaining sub-solidus HTLP metamorphism and metasomatism in rocks adjacent to the main channel of the shear zone.

Pulses of hot fluid travelling up and emanating from this main conduit migrated laterally and vertically through vein networks and porous horizons into adjacent metasedimentary rocks (Figure 9b). While Aberfoyle remained below the solidus, progressive heating through the core of the system (*i.e.* within the highest strain rocks that experienced the highest fluid/melt flux) formed migmatite and a switch to melt-present deformation and advection of magma (Jessop *et al.*, 2025).

Conclusions

Detailed geological mapping at Aberfoyle identifies five metasedimentary units that define a systematic progression in metamorphic grade from greenschist to amphibolite facies. This progression, developed adjacent to a quartzite unit containing amphibolite pods, closely mirrors that observed at Lyndhurst-Rosewood on the margins of the WSZ.

HTLP metamorphism at Aberfoyle was driven by fluid advected heat rather than local magmatism. The absence of exposed plutonic bodies at Aberfoyle, coupled with the steep metamorphic field gradient developed over ~1 km, requires a mechanism for heat transfer other than local magmatic intrusion. We conclude that metamorphism was initiated and sustained by advected heat carried by hot fluids derived from deeper levels of the metasedimentary rock pile during early Permian crustal extension and channelled up the WSZ.

Metamorphism was accompanied by extensive metasomatism evidenced by systematic enrichment or depletion of fluid-mobile elements with metamorphic grade. These trends, together with petrographic evidence for progressive replacement of plagioclase by biotite and K-feldspar, indicate open-system behaviour and significant fluid–rock interaction. Disturbance of the Sr isotopic system and increasing $\delta^{18}O$ values with grade further support metasomatism mediated by hot fluids.

Veining and deformation record a fluid-rich, syn-tectonic metamorphic system. The generally progressive increase in foliation intensity, vein density and vein complexity with metamorphic grade demonstrates that fluid flow was closely coupled to deformation. Channelised flow through vein networks, enhanced permeability along lithological and rheological boundaries, and growth of metamorphic porphyroblasts along deformation-related cracks indicate that fluids migrated both along shear zones and through the rock matrix during deformation.

Fluid flow was locally pulsed but regionally sustained. Petrographic relationships and mineral chemistry, particularly the coexistence of preserved and retrogressed cordierite and subtle prograde–retrograde chemical signatures in biotite and muscovite, indicate that fluid flux occurred in pulses at the outcrop scale. However, the persistence of the metamorphic field gradient and systematic metasomatism require that, at the scale of the rock package, fluid flux was effectively continuous over the duration of metamorphism.

Overall, this study demonstrates that sustained, pulsed, hot, metamorphic fluids can initiate steep HTLP metamorphic field gradients in the absence of direct magmatism. The Aberfoyle sequence provides a clear example of how extension-driven fluid flow along major shear zones can transfer heat and mass into adjacent crustal blocks, producing spatially organised metamorphism and sub-regional scale metasomatism.

Acknowledgements

Landowners at Wongwibinda and Aberfoyle are thanked for providing help and access to their properties. The generosity of Dr Terry Farrell in providing data and samples from his previous work at Wongwibinda is also fully appreciated. The input from Dr Ioan Stanislav and an anonymous reviewer has greatly enhanced the content and clarity of the manuscript.

Author contributions

CRediT: **K. Jessop**: Investigation, Writing – original draft, Writing – review & editing. **N. R. Daczko**: Conceptualisation, Writing - review & editing. **S. Piazolo**: Conceptualisation: Writing - review & editing.

Disclosure statement

No potential conflict of interest was reported by the authors.

ORCID

K. Jessop http://orcid.org/0000-0001-6921-3942
N. R. Daczko http://orcid.org/0000-0002-3737-3818
S. Piazolo http://orcid.org/0000-0001-7723-8170

Data availability statement

All new data used here are contained within the paper, figures and Supplemental data.

References

Ague, J. J. (2003). Fluid flow in the deep crust. In R. L. Rudnick (Ed.), *Treatise on geochemistry* (pp. 195–228). Elsevier.

Ague, J. J. (2011). Extreme channelization of fluid and the problem of element mobility during Barrovian metamorphism. *American Mineralogist*, *96*(2-3), 333–352. https://doi.org/10.2138/am.2011.3582

Ague, J. J. (2017). Element mobility during regional metamorphism in crustal and subduction zone environments with a focus on the rare earth elements (REE). *American Mineralogist*, *102*(9), 1796–1821. https://doi.org/10.2138/am-2017-6130

Alcott, J. R. (1979). *The high-grade Rampsbeck Schists, migmatites and gneiss of the Wongwibinda Metamorphic Complex* [Unpublished 3rd Year Project]. University of New England.

Austrheim, H. (2013). Fluid and deformation induced metamorphic processes around Moho beneath continent collision zones: Examples from the exposed root zone of the Caledonian mountain belt, W-Norway. *Tectonophysics*, *609*, 620–635. https://doi.org/10.1016/j.tecto.2013.08.030

Bickle, M. J., & McKenzie, D. (1987). The transport of heat and matter by fluids during metamorphism. *Contributions to Mineralogy and Petrology*, *95*(3), 384–392. https://doi.org/10.1007/BF00371852

Binns, R. A. (1966). Granitic intrusions and regional metamorphic rocks of Permian age from the Wongwibinda district, north-eastern New South Wales. *Journal and Proceedings of the Royal Society of NSW*, *99*, 5–36. https://www.biodiversitylibrary.org/page/46313253#page/17/mode/1up

Binns, R. A., & Richards, J. R. (1965). Regional metamorphic rocks of Permian age from the New England district of New South Wales. *Australian Journal of Science*, *27*, 233.

Bodorkos, S., Sandiford, M., Oliver, N. H. S., & Cawood, P. A. (2002). High-T, low-P metamorphism in the Palaeoproterozoic Halls Creek Orogen, northern Australia: The middle crustal response to a mantle-related transient thermal pulse. *Journal of Metamorphic Geology*, *20*(2), 217–237. https://doi.org/10.1046/j.1525-1314.2002.00339.x

Bons, P. D., & Gomez-Rivas, E. (2020). Origin of meteoric fluids in extensional detachments. *Geofluids*, *2020*, 1–8. https://doi.org/10.1155/2020/7201545

Buttigieg, J. (1984). *Aspects of the metamorphic geology on the properties of Noorilim and Lynoch, (Wongwibinda) sixty kilometres Northeast of Armidale, Northeastern New South Wales* [Unpublished 3rd Year Project]. University of New England.

Cawood, P. A. (1982). Structural relations in the subduction complex of the Paleozoic New England Fold Belt, eastern Australia. *The Journal of Geology*, *90*(4), 381–392. https://doi.org/10.1086/628692

Cawood, P. A. (1983). Modal composition and detrital clinopyroxene geochemistry of lithic sandstones from the New England Fold Belt (east Australia): A Paleozoic forearc terrane. *Geological Society of America Bulletin*, *94*(10), 1199–1214. https://doi.org/10.1130/0016-7606(1983)94≤1199:MCADCG≥2.0.CO;2

Cawood, P. A. (1984). A geochemical study of metabasalts from a subduction complex in eastern Australia. *Chemical Geology*, *43*(1-2), 29–47. https://doi.org/10.1016/0009-2541(84)90139-6

Clerc, C., Lahfid, A., Monié, P., Lagabrielle, Y., Chopin, C., Poujol, M., Boulvais, P., Ringenbach, J-C., Masini, E., & de St Blanquat, M. (2015). High-temperature metamorphism during extreme thinning of the continental crust: A reappraisal of the North Pyrenean passive paleomargin. *Solid Earth*, *6*(2), 643–668. https://doi.org/10.5194/se-6-643-2015

Cox, S. F. (2007). Structural and isotopic constraints on fluid flow regimes and fluid pathways during upper crustal deformation: An example from the Taemas area of the Lachlan Orogen, SE Australia. *Journal of Geophysical Research: Solid Earth*, *112*(B8), B08208. https://doi.org/10.1029/2006JB004734

Craven, S. J. (2015). *The evolution of the Wongwibinda high-T–low-P metamorphic complex* [Unpublished PhD thesis]. Macquarie University.

Craven, S. J., Daczko, N. R., & Halpin, J. A. (2012). Thermal gradient and timing of high-T–low-P metamorphism in the Wongwibinda Metamorphic Complex, southern New England Orogen, Australia. *Journal of Metamorphic Geology*, *30*(1), 3–20. https://doi.org/10.1111/j.1525-1314.2011.00949.x

Craven, S. J., Daczko, N. R., & Halpin, J. A. (2013). High-T–low-P thermal anomalies superposed on biotite-grade rocks, Wongwibinda Metamorphic Complex, southern New England Orogen, Australia: Heat advection by aqueous fluid? *Australian Journal of Earth Sciences*, *60*(5), 621–635. https://doi.org/10.1080/08120099.2013.814590

Danis, C. (2007). *The Wongwibinda Complex, New England Fold Belt: A tilted low-P high-T terrane?* [Unpublished BSc Honours Thesis]. Macquarie University.

Danis, C. R., Daczko, N. R., Lackie, M. A., & Craven, S. J. (2010). Retrograde metamorphism of the Wongwibinda Complex, New England Fold Belt and the implications of 2.5 D subsurface geophysical structure for the metamorphic history. *Australian Journal of Earth Sciences*, *57*(3), 357–375. https://doi.org/10.1080/08120091003678361

Daczko, N. R., & Halpin, J. A. (2009). Evidence for melt migration enhancing recrystallization of metastable assemblages in mafic lower crust, Fiordland, New Zealand. *Journal of Metamorphic Geology*, *27*(2), 167–185. https://doi.org/10.1111/j.1525-1314.2009.00811.x

Dipple, G. M., & Ferry, J. M. (1992). Metasomatism and fluid flow in ductile fault zones. *Contributions to Mineralogy and Petrology*, *112*(2-3), 149–164. https://doi.org/10.1007/BF00310451

Doyle, C., & Cartwright, I. (2000). The role of fluids in retrograde shearing: Broken Hill, Australia. *Journal of Geochemical Exploration*, *69*, 575–579. https://doi.org/10.1016/S0375-742(00)00062-5

England, P. C., & Thompson, A. B. (1984). Pressure—temperature—time paths of regional metamorphism I. Heat transfer during the evolution of regions of thickened continental crust. *Journal of Petrology*, *25*(4), 894–928. https://doi.org/10.1093/petrology/25.4.894

Evans, K. A., & Tomkins, A. G. (2020). The role of fluids in retrograde shearing: Broken Hill, Australia2020). Metamorphic fluids in orogenic settings. *Elements*, *16*(6), 381–387. https://doi.org/10.2138/gselements.16.6.381

Farmer, M. (2017). *Migmatite delineates zones of melt flux through the upper crust, Wongwibinda, NSW* [Unpublished masters thesis]. Macquarie University.

Farrell, T. R. (1992). *Deformation, metamorphism and migmatite genesis in the Wongwibinda Metamorphic Complex, Eastern Australia* [Unpublished PhD thesis]. University of Newcastle.

Faure, G., & Hensing, T. M. (2005). *Isotopes: Principles and applications* (3rd ed.). Wiley.

Ferry, J. M. (1988). Contrasting mechanisms of fluid flow through adjacent stratigraphic units during regional metamorphism, south-central Maine, USA. *Contributions to Mineralogy and Petrology*, *98*(1), 1–12. https://doi.org/10.1007/BF00371903

Ferry, J. M. (1994). A historical review of metamorphic fluid flow. *Journal of Geophysical Research: Solid Earth*, *99*(B8), 15487–15498. https://doi.org/10.1029/94JB01147

Ferry, J. M., & Dipple, G. M. (1991). Fluid flow, mineral reactions, and metasomatism. *Geology*, *19*(3), 211–214. https://doi.org/10.1130/0091-7613(1991)019≤0211:Ffmram≥2.3.Co;2

Ferry, J. M., Winslow, N. W., & Penniston-Dorland, S. C. (2013). Re-evaluation of infiltration-driven regional metamorphism in northern New England: New transport models with solid solution and cross-layer equilibration of fluid composition. *Journal of Petrology*, *54*(12), 2455–2485. https://doi.org/10.1093/petrology/egt053

Fisher, D. (1968). *A structural analysis and some aspects of the metamorphic petrology of the Little Chandler River Area, Wongwibinda* [Unpublished 3rd Year Project]. University of New England.

Flood, R. H., & Vernon, R. H. (1978). The Cooma Granodiorite, Australia: An example of in situ crustal anatexis? *Geology*, *6*(2), 81–84. https://doi.org/10.1130/0091-7613(1978)6≤81:TCGAAE≥2.0.CO;2

Fusseis, F., Regenauer-Lieb, K., Liu, J., Hough, R., & De Carlo, F. (2009). Creep cavitation can establish a dynamic granular fluid pump in ductile shear zones. *Nature*, *459*(7249), 974–977. https://doi.org/10.1038/nature08051

Gates, A. E., & Speer, J. A. (1991). Allochemical retrograde metamorphism in shear zones: An example in metapelites, Virginia, USA. *Journal of Metamorphic Geology*, *9*(5), 581–604. https://doi.org/10.1111/j.1525-1314.1991.tb00550.x

Henson, A. (2000). *EMP and LA-ICP-MS raster analysis: A new method for analysing fine-grained sediments? And a geochemical study of the metasediments of the Wongwibinda Metamorphic Complex* [Unpublished BSc honours thesis]. Macquarie University.

Ingebritsen, S. E., Sanford, W. E., & Neuzil, C. E. (2006). *Groundwater in geologic processes*. Cambridge University Press.

Jackson, R. A. (1987). *The geology of the Wards Mistake Area (Wongwibinda)* [Unpublished 3rd Year Project]. University of New England.

Jamtveit, B., Austrheim, H., & Malthe-Sørenssen, A. (2000). Accelerated hydration of the Earth's deep crust induced by stress perturbations. *Nature*, *408*(6808), 75–78. https://doi.org/10.1038/35040537

Jeon, H., Williams, I. S., & Chappell, B. W. (2012). Magma to mud to magma: Rapid crustal recycling by Permian granite magmatism near the eastern Gondwana margin. *Earth and Planetary Science Letters*, *319-320*, 104–117. https://doi.org/10.1016/j.epsl.2011.12.010

Jessop, K. (2017). *The role of aqueous fluids in regional-style HTLP metamorphism* [Unpublished PhD thesis]. Macquarie University.

Jessop, K., Daczko, N. R., & Piazolo, S. (2019). Tectonic cycles of the New England Orogen, Eastern Australia: A review. *Australian Journal of Earth Sciences*, *66*(4), 459–496. https://doi.org/10.1080/08120099.2018.1548378

Jessop, K., Daczko, N. R., & Piazolo, S. (2020a). Metamorphism in the New England Orogen, eastern Australia: A review. *Australian Journal of Earth Sciences*, *67*(4), 453–478. https://doi.org/10.1080/08120099.2020.1685000

Jessop, K., Daczko, N. R., & Piazolo, S. (2020b). Two belts of HTLP sub-regional metamorphism in the New England Orogen, eastern Australia: Occurrence and characteristics exemplified by the Wongwibinda Metamorphic Complex. *Australian Journal of Earth Sciences*, *67*(4), 479–507. https://doi.org/10.1080/08120099.2019.1698275

Jessop, K., Daczko, N., & Piazolo, S. (2025). Occurrence and petrogenesis of diverse S-type granites in an extensional tectonic setting: A case study from the Wongwibinda Complex, eastern Australia. *Australian Journal of Earth Sciences*, *72*(2), 213–232. https://doi.org/10.1080/08120099.2025.2476519

Korsch, R. J. (1981). Structural geology of the Rockvale block, northern New South Wales. *Journal of the Geological Society of Australia*, *28*(1-2), 51–70. https://doi.org/10.1080/00167618108729143

Korsch, R. J., Totterdell, J. M., Cathro, D. L., & Nicoll, M. G. (2009). Early Permian East Australian Rift System. *Australian Journal of Earth Sciences*, *56*(3), 381–400. https://doi.org/10.1080/08120090802698703

Landenberger, W., & Collins, W. (1996). Derivation of A-type granites from a dehydrated charnockitic lower crust: Evidence from the Chaelundi Complex, Eastern Australia. *Journal of Petrology*, *37*(1), 145–170. https://doi.org/10.1093/petrology/37.1.145

Langmuir, C. H., Vocke, R. D., Jr., Hanson, G. N., & Hart, S. R. (1978). A general mixing equation with applications to Icelandic basalts. *Earth and Planetary Science Letters*, *37*(3), 380–392. https://doi.org/10.1016/0012-821X(78)90053-5

Langone, A., Godard, G., Prosser, G., Caggianelli, A., Rottura, A., & Tiepolo, M. (2010). P–T–t path of the Hercynian low-pressure rocks from the Mandatoriccio complex (Sila Massif, Calabria, Italy): New insights for crustal evolution. *Journal of Metamorphic Geology*, *28*(2), 137–162. https://doi.org/10.1111/j.1525-1314.2009.00858.x

Lewerentz, A., & Skelton, A. D. (2018). Fluid and carbon flux estimation of regional metamorphic fluid flow in Glen Esk, SE Scottish Highlands: The role of hydrodynamic dispersion for broadening of an isotopic front. *American Journal of Science*, *318*(4), 435–457. https://doi.org/10.2475/04.2018.03

Lewerentz, A., Skelton, A. D. L., Linde, J. K., Nilsson, J., Möller, C., Crill, P. M., & Spicuzza, M. J. (2017). On the association between veining and index mineral distributions in Barrow's Metamorphic Zones, Glen Esk, Scotland. *Journal of Petrology*, *58*(5), 885–907. https://doi.org/10.1093/petrology/egx039

McCarron, J. (1989). *Fishington: A study of the structural, petrographic and metamorphic features of a part of the Wongwibinda Metamorphic Complex, NSW* [Unpublished 3rd Year Project]. University of New England.

Oliver, N. H. S. (1996). Review and classification of structural controls on fluid flow during regional metamorphism. *Journal of Metamorphic Geology*, *14*(4), 477–492. https://doi.org/10.1046/j.1525-1314.1996.00347.x

Passchier, C. W. (1991). Geometric constraints on the development of shear bands in rocks. *Netherlands Journal of Geosciences*, *70*, 203–211.

Rollinson, H. (1993). *Using geochemical data: Evaluation, presentation, interpretation*. Pearson Education, Prentice Hall.

Sandiford, M., & Powell, R. (1986). Deep crustal metamorphism during continental extension: Modern and ancient examples. *Earth and Planetary Science Letters*, *79*(1-2), 151–158. https://doi.org/10.1016/0012-821X(86)90048-8

Sandiford, M., Hand, M., & McLaren, S. (1998). High geothermal gradient metamorphism during thermal subsidence. *Earth and Planetary Science Letters*, *163*(1-4), 149–165. https://doi.org/10.1016/S0012-821X(98)00183-6

Sanislav, I. V., Abu Sharib, A. S. A. A., & Quentin de Gromard, R. S. A. (2020). Deformation-induced cordierite breakdown—An example from western Maine, USA. *Journal of Metamorphic Geology*, *38*(8), 831–852. https://doi.org/10.1111/jmg.12551

Siron, G., Bodner, R., Baumgartner, L., Putlitz, B., & Vennemann, T. (2021). Limited channelized fluid infiltration in the Torres del Paine contact aureole. *American Mineralogist*, *106*(9), 1453–1469. https://doi.org/10.2138/am-2021-7622

Steele-MacInnis, M., & Manning, C. E. (2020). Hydrothermal properties of geologic fluids. *Elements*, *16*(6), 375–380. https://doi.org/10.2138/gselements.16.6.375

Stephenson, N. C. N., & Hensel, H. D. (1979). Intergrown calcic and Fe-Mg amphiboles from the Wongwibinda Metamorphic Complex., N.S.W., Australia. *Canadian Mineralogist*, *17*, 11–23.

Stephenson, N. C. N., & Hensel, H. D. (1982). Amphibolites and related rocks from the Wongwibinda metamorphic complex, northern N.S.W., Australia. *Lithos*, *15*(1), 59–75. https://doi.org/10.1016/S0024-4937(82)80006-6

Stuart, C. A. (2012). *Aqueous fluid advection: A plausibe mechanism for heating the shallow crust to form HTLP metamorphic belts* [Unpublished BSc honours thesis]. Macquarie University.

Sun, S. S., & McDonough, W. F. (1989). Chemical and isotopic systematics of oceanic basalts: Implications for mantle composition and processes. In A. D. N. Saunders & M. J. Norry (Eds.), *Magmatism in ocean basins* (Vol. 42, pp. 313–345). Geological Society of London Special Publication. https://doi.org/10.1144/GSL.SP.1989.042.01.19

Teague, E. (2010). *A geochronological assessment into the evolution of the Wongwibinda Complex, Southern New England Fold Belt* [Unpublished BSc honours thesis]. Macquarie University.

Tian, M., Ague, J. J., Chu, X., Baxter, E. F., Dragovic, N., Chamberlain, C. P., & Rumble, D., III. (2018). The potential for metamorphic thermal pulses to develop during compaction-driven fluid flow. *Geochemistry, Geophysics, Geosystems*, *19*(1), 232–256. https://doi.org/10.1002/2017GC007269

Vernon, R. H. (1982). Isobaric cooling of two regional metamorphic complexes related to igneous intrusions in southeastern Australia. *Geology*, *10*(2), 76. https://doi.org/10.1130/0091-7613(1982)10≤76:Icotrm≥2.0.co;2

Wickham, S. M., & Oxburgh, E. R. (1985). Continental rifts as a setting for regional metamorphism. *Nature*, *318*(6044), 330–333. https://doi.org/10.1038/318330a0

Yardley, B. W., & Cleverley, J. S. (2015). The role of metamorphic fluids in the formation of ore deposits. In G. R. T. Jenkin, P. A. J. Lusty, I. McDonald, M. P. Smith, A. J. Boyce, & J. J. Wilkinson (Eds.), *Ore deposits in an evolving earth* (Vol. 393, pp. 117–134). Geological Society of London Special Publications. https://doi.org/10.1144/SP393.5

Yardley, B. W. D. (2013). The chemical composition of metasomatic fluids in the crust. In *Metasomatism and the chemical transformation of rock* (pp. 17–51). Springer. https://doi.org/10.1007/978-3-642-28394-9_2

Yardley, B. W. D., & Bodnar, R. J. (2014). Fluids in the continental crust. *Geochemical Perspectives*, *3*(1), 1–127. https://doi.org/10.7185/geochempersp.3.1